

# Supporting Information for

## **Sequestration of guest intermediates by dalesconol bioassembly lines in *Daldinia eschscholzii***

Ai Hua Zhang, Wen Liu, Nan Jiang, Xin Lei Wang, Gang Wang, Qiang Xu, and Ren Xiang Tan\*

\*Corresponding author. E-mail: [rxtan@nju.edu.cn](mailto:rxtan@nju.edu.cn).

### **Table of Contents**

Material and Methods .....	2–5
Supplementary tables .....	6–11
References .....	12
Supplementary figures .....	13–44

## Materials and methods

### Fungal cultivation and fractionation

*D. eschscholzii* IFB-TL01<sup>1-3</sup> was cultured on slants of potato dextrose agar (PDA) at 25 °C for 5 days. The fresh mycelium taken from the fungal colony in the Petri dish was inoculated into flasks (always 1 L size). To each 400 mL of medium (20 g/L malt extract, 20 g/L sucrose, 1 g/L peptone) in flasks, procaine (90 mg) dissolved appropriately in sterilized water were added at 24, 48 and 72 h after inoculation (each 30 mg), followed by 15-day fermentation at 25 °C with agitation (200 rpm). The broth was collected and extracted with EtOAc. *In vacuo* evaporation of solvent from the extract gave a residue which was subjected to column chromatography (CC) over silica gel (300–400 mesh, 50 × 15 cm) eluted with the CH<sub>2</sub>Cl<sub>2</sub>/MeOH mixture (v/v 100:0, 100:1, 100:2, 100:4) to afford four CC fractions F1–F4. The CC fractions of interest were separated by gel filtration over Sephadex LH-20, and semipreparative HPLC (if necessary). Gel filtration of F3 over Sephadex LH-20 in MeOH gave **13** (33.7 mg, yellow powder) and **19** (0.8 mg, yellow powder) from the solvent and a mixture which afforded **14** (6.8 mg, brown powder) and **15** (3.8 mg, brown powder) by semi-preparative HPLC separation utilizing 76% MeOH in H<sub>2</sub>O. F4 was processed in same way to give **16** (2.1 mg, red powder), **17** (1.3 mg, red powder), and **18** (1.5 mg, red powder) by final semi-preparative HPLC separation using 60% MeOH in H<sub>2</sub>O.

### Structure elucidation

Dalescone B (**14**) was evidenced to have a molecular formula of C<sub>30</sub>H<sub>20</sub>O<sub>7</sub> from the Na<sup>+</sup>-liganded molecular ion at *m/z* 515.10991 (calcd 515.1101) in its HR-ESI-MS spectrum. This observation, along with its <sup>1</sup>H- and <sup>13</sup>C-NMR spectra, suggested that it was probably hydroxymethylated dalesconol A.<sup>1</sup> This proposal was confirmed by its single crystal X-ray diffraction, which disclosed simultaneously its relative configuration (Figure S2). The enantiomers of **14** were obtained by chiral HPLC resolution, and the absolute configuration of (+)-**14** and (–)-**14** was elucidated to be 19*S*,28*S* and 19*R*,28*R*, respectively, according to their CD curves that match perfectly to those of (+)-**13** and (–)-**13** (Figure S28).

Dalescone C (**15**) was demonstrated to share the same molecular formula (C<sub>30</sub>H<sub>20</sub>O<sub>7</sub>) with that of **3** by the Na<sup>+</sup>-liganded molecular ion at *m/z* 515.11002 (calcd 515.1101) in its HR-ESI-MS spectrum. In the <sup>1</sup>H-NMR signals of **15**, a pair of H-30 doublets (*J* = 14.8 Hz) at δ<sub>H</sub> 4.80 and 4.77, showing the HMBC correlations with C-10 and C-12, indicated that it was a 11-hydroxymethylated dalesconol A.<sup>1</sup> The structure of **15** was reinforced by its single crystal X-ray diffraction (Figure S3). Chiral HPLC separation of **15** gave (+)-**15** and (–)-**15**, which were shown to share the same absolute configurations with those of (+)-**14** (19*S*,28*S*) and (–)-**14** (19*R*,28*R*), respectively (Figure S36).

Dalescone D (**16**) was evidenced to have a molecular formula of C<sub>31</sub>H<sub>22</sub>O<sub>7</sub> from the Na<sup>+</sup>-liganded molecular ion at *m/z* 529.1255 (calcd 529.1258) in its HR-ESI-MS spectrum. The <sup>1</sup>H- and <sup>13</sup>C-NMR spectra of **16** suggested its skeletal resemblance to **15**. However, the 11-hydroxymethyl NMR signals of **15** were replaced by a 2-hydroxyethyl group of **16**, resonating at δ<sub>C</sub> 67.1 (CH) and 23.1 (CH<sub>3</sub>), and at δ<sub>H</sub> 5.12 (q, *J* = 6.4 Hz) and 1.63 (d, *J* = 6.4 Hz). This assignment was substantiated by the single crystal X-ray crystallographic analysis which addressed as well its relative configuration (Figures S4 and S5). To clarify the absolute stereochemistry for each enantiomer of **16**, chiral HPLC separation was performed to yield four

enantiomers (+)-**16a** (19*S*,28*S*,30*S*), (–)-**16a** (19*R*,28*R*,30*R*) (+)-**16b** (19*S*,28*S*,30*R*) and (–)-**16b** (19*R*,28*R*,30*S*) with the configurations ascertained by comparing the recorded CD curves with the ECD spectra simulated theoretically for all optional isomers (Figures S45 and S47).

Dalescone E (**17**) was demonstrated to have a molecular formula of C<sub>31</sub>H<sub>22</sub>O<sub>8</sub> by the protonated molecular ion at *m/z* 523.1391 (calcd 523.1387) in its HR-ESI-MS spectrum. The <sup>1</sup>H-NMR spectrum of **17** was close to that of dalescone D (**16**). The structure assignment, together with the relative stereochemistry of **17**, was unequivocally addressed by its single crystal X-ray diffraction analysis (Figure 5). Subsequent chiral HPLC separation and CD curves with those of calculated ECD spectra corroborated collectively that (+)-**17** and (–)-**17** have 19*S*,28*S*,30*R* and 19*R*,28*R*,30*S*-configurations, respectively (Figure S54).

Dalescone F (**18**) was determined to have a molecular formula of C<sub>30</sub>H<sub>20</sub>O<sub>8</sub> (an oxygen atom extra over that of **15**) by the protonated molecular ion at *m/z* 509.1225 (calcd 509.1231) in its HR-ESI-MS spectrum. The <sup>1</sup>H-NMR signals of **18** was well comparable to that of **15**, but failed to display the triplet of H-5 at δ<sub>H</sub> 7.46 (*J* = 8.0 Hz) discerned in that of **15**. These spectral data highlighted the presence of 5-hydroxyl group in the structure of **18**. Since **18** was obtained as a racemic mixture, chiral HPLC separation was performed to give two enantiomers (+)-**18** and (–)-**18**, which were shown to share the same absolute configurations with those of (+)-**15** (19*S*,28*S*) and (–)-**15** (19*R*,28*R*), respectively (Figure S59).

Dalescone G (**19**) was shown to possess a molecular formula of C<sub>32</sub>H<sub>22</sub>O<sub>8</sub> corresponding to the protonated molecular ion at *m/z* 535.1386 (calcd 535.1387) in its HR-ESI-MS spectrum. This observation, along with its <sup>1</sup>H-NMR spectra, suggested that it was probably methoxylated **13**. This proposal was confirmed by its single crystal X-ray diffraction, which disclosed simultaneously its relative configuration (Figure S6). Chiral HPLC separation of **19** was performed to yield four enantiomers (+)-**19a** (19*S*,28*S*,30*R*), (–)-**19a** (19*R*,28*R*,30*S*) (+)-**19b** (19*S*,28*S*,30*S*) and (–)-**19b** (19*R*,28*R*,30*R*) with the configurations ascertained by comparing the recorded CD curves with the calculated ECD spectra for all possible stereoisomers (Figures S64 and S65).

## X-ray crystallographic diffractions

The structures were solved by direct methods (SHELXS-97) and refined using full-matrix least-squares difference Fourier techniques. Crystallographic data in CIF format have been deposited in the Cambridge Crystallographic Data Centre [available free of charge at <http://www.ccdc.cam.ac.uk/deposit> or from the CCDC, 12 Union Road, Cambridge CB21EZ, UK; fax: (+44) 1223-336-033; or e-mail: [deposit@ccdc.cam.ac.uk](mailto:deposit@ccdc.cam.ac.uk)].

### Crystal data

Dalescone A (**13**): Diffraction measurements were performed at 100 K on an Agilent SuperNova diffractometer equipped with Cu–K<sub>α</sub> radiation ( $\lambda$  = 1.54184 Å). C<sub>31</sub>H<sub>20</sub>O<sub>7</sub>, *M<sub>r</sub>* = 536.51, monoclinic, space group *P*2<sub>1</sub>/*n*, *a* = 8.5702(2) Å, *b* = 19.8368(8) Å, *c* = 13.8839(5) Å, *V* = 2354.86(14) Å<sup>3</sup>, *Z* = 4, *D<sub>x</sub>* = 1.513 g/cm<sup>3</sup>,  $\mu$  = 0.904 mm<sup>–1</sup> and *F*(000) = 1120.0; crystal dimensions: 0.30 × 0.30 × 0.03 mm<sup>3</sup>; 3870 unique reflections with 4869 obeying the *I* ≥ 2σ(*I*); *R*1 = 0.0449, *wR*2 = 0.148, *S* = 1.024; supplementary publication no.CCDC-1015012.

Dalescone B (**14**): Diffraction measurements were performed at 296 K on an Agilent

SuperNova diffractometer equipped with Cu- $K_\alpha$  radiation ( $\lambda = 1.54178 \text{ \AA}$ ).  $C_{30}H_{20}O_7$ ,  $M_r = 492.46$ , triclinic, space group  $P-1$ ,  $a = 7.3385(2) \text{ \AA}$ ,  $b = 11.9720(3) \text{ \AA}$ ,  $c = 13.1171(3) \text{ \AA}$ ,  $V = 1121.06(5) \text{ \AA}^3$ ,  $Z = 2$ ,  $D_x = 1.459 \text{ g/cm}^3$ ,  $\mu = 0.863 \text{ mm}^{-1}$  and  $F(000) = 512.0$ ; crystal dimensions:  $0.25 \times 0.23 \times 0.11 \text{ mm}^3$ ; 3151 unique reflections with 3691 obeying the  $I \geq 2\sigma(I)$ ;  $R1 = 0.053$ ,  $wR2 = 0.163$ ,  $S = 1.054$ ; supplementary publication no.CCDC-1015013.

Dalescone C (15): Diffraction measurements were performed at 100 K on an Agilent SuperNova diffractometer equipped with Mo- $K_\alpha$  radiation ( $\lambda = 0.71073 \text{ \AA}$ ).  $C_{30}H_{20}O_7$ ,  $M_r = 492.46$ , monoclinic, space group  $P2_1/n$ ,  $a = 14.1170(9) \text{ \AA}$ ,  $b = 8.1361(4) \text{ \AA}$ ,  $c = 22.5808(14) \text{ \AA}$ ,  $V = 2585.3(3) \text{ \AA}^3$ ,  $Z = 4$ ,  $D_x = 1.265 \text{ g/cm}^3$ ,  $\mu = 0.091 \text{ mm}^{-1}$  and  $F(000) = 1024.0$ ; crystal dimensions:  $0.40 \times 0.20 \times 0.10 \text{ mm}^3$ ; 3762 unique reflections with 5979 obeying the  $I \geq 2\sigma(I)$ ;  $R1 = 0.064$ ,  $wR2 = 0.192$ ,  $S = 1.084$ ; supplementary publication no.CCDC-1015014.

Dalescone D (16a): Diffraction measurements were performed at 100 K on an Agilent SuperNova diffractometer equipped with Cu- $K_\alpha$  radiation ( $\lambda = 1.54184 \text{ \AA}$ ).  $C_{31}H_{22}O_7$ ,  $M_r = 506.49$ , monoclinic, space group  $P2_1/n$ ,  $a = 10.4921(1) \text{ \AA}$ ,  $b = 20.6042(1) \text{ \AA}$ ,  $c = 11.3125(1) \text{ \AA}$ ,  $V = 2268.80(4) \text{ \AA}^3$ ,  $Z = 4$ ,  $D_x = 1.483 \text{ g/cm}^3$ ,  $\mu = 0.869 \text{ mm}^{-1}$  and  $F(000) = 1056.0$ ; crystal dimensions:  $0.30 \times 0.20 \times 0.05 \text{ mm}^3$ ; 4443 unique reflections with 4766 obeying the  $I \geq 2\sigma(I)$ ;  $R1 = 0.045$ ,  $wR2 = 0.129$ ,  $S = 1.022$ ; supplementary publication no.CCDC-1015015.

Dalescone D (16b): Diffraction measurements were performed at 100 K on an Agilent SuperNova diffractometer equipped with Cu- $K_\alpha$  radiation ( $\lambda = 1.54184 \text{ \AA}$ ).  $C_{31}H_{22}O_7$ ,  $M_r = 506.49$ , monoclinic, space group  $P2_1/c$ ,  $a = 13.7367(1) \text{ \AA}$ ,  $b = 8.5632(1) \text{ \AA}$ ,  $c = 19.5622(2) \text{ \AA}$ ,  $V = 2280.37(4) \text{ \AA}^3$ ,  $Z = 4$ ,  $D_x = 1.475 \text{ g/cm}^3$ ,  $\mu = 0.865 \text{ mm}^{-1}$  and  $F(000) = 1056.0$ ; crystal dimensions:  $0.40 \times 0.40 \times 0.20 \text{ mm}^3$ ; 4514 unique reflections with 4778 obeying the  $I \geq 2\sigma(I)$ ;  $R1 = 0.044$ ,  $wR2 = 0.121$ ,  $S = 1.008$ ; supplementary publication no.CCDC-1015016.

Dalescone E (17): Diffraction measurements were performed at 100 K on an Agilent SuperNova diffractometer equipped with Cu- $K_\alpha$  radiation ( $\lambda = 1.54184 \text{ \AA}$ ).  $C_{31}H_{26}O_{10}$ ,  $M_r = 558.52$ , monoclinic, space group  $P2_1$ ,  $a = 8.3894(4) \text{ \AA}$ ,  $b = 14.6187(8) \text{ \AA}$ ,  $c = 10.2645(4) \text{ \AA}$ ,  $V = 1247.76(4) \text{ \AA}^3$ ,  $Z = 2$ ,  $D_x = 1.487 \text{ g/cm}^3$ ,  $\mu = 0.937 \text{ mm}^{-1}$  and  $F(000) = 584.0$ ; crystal dimensions:  $0.15 \times 0.10 \times 0.05 \text{ mm}^3$ ; 4538 unique reflections with 5057 obeying the  $I \geq 2\sigma(I)$ ;  $R1 = 0.037$ ,  $wR2 = 0.098$ ,  $S = 1.033$ ; supplementary publication no.CCDC-1498041.

Dalescone G (19): Diffraction measurements were performed at 296 K on an Agilent SuperNova diffractometer equipped with Cu- $K_\alpha$  radiation ( $\lambda = 1.54178 \text{ \AA}$ ).  $C_{32}H_{22}O_8$ ,  $M_r = 534.50$ , monoclinic, space group  $P2_1/c$ ,  $a = 7.4426(3) \text{ \AA}$ ,  $b = 20.2962(10) \text{ \AA}$ ,  $c = 16.8662(8) \text{ \AA}$ ,  $V = 2540.3(2) \text{ \AA}^3$ ,  $Z = 4$ ,  $D_x = 1.398 \text{ g/cm}^3$ ,  $\mu = 0.838 \text{ mm}^{-1}$  and  $F(000) = 1112.0$ ; crystal dimensions:  $0.21 \times 0.18 \times 0.11 \text{ mm}^3$ ; 2902 unique reflections with 4187 obeying the  $I \geq 2\sigma(I)$ ;  $R1 = 0.061$ ,  $wR2 = 0.120$ ,  $S = 1.013$ ; supplementary publication no.CCDC-1498042.

## ECD calculation details

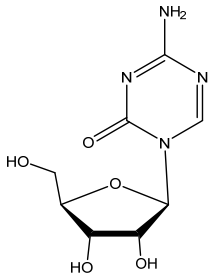
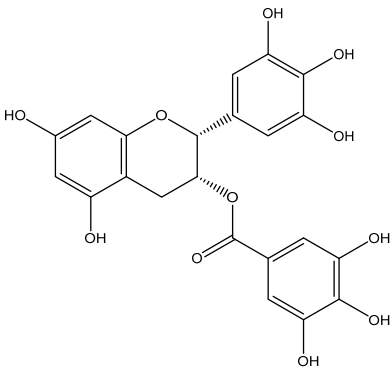
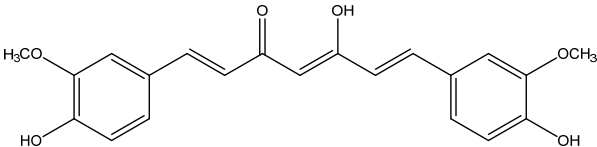
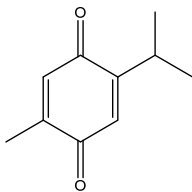
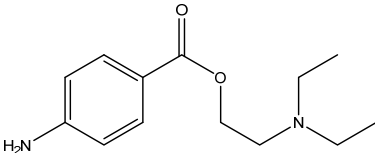
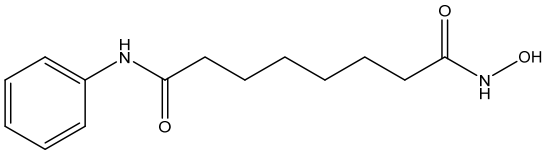
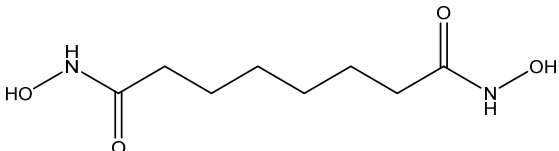
The density functional theory (DFT) at B3LYP/6–31G (d, p) level was employed to optimize the geometries of the studied systems, taking crystal structures as the original conFigureation. The solvent effects on the electronic structures of the concerned systems were evaluated by quantum chemistry method through the polarizable continuum model (PCM, dielectric constant  $\epsilon = 32.64$  for  $CH_3OH$ ). Then, the corresponding excited-state calculations were performed at the ground-state optimized geometries. Time-dependent DFT in combination with PCM model (TD-DFT/PCM) with the same basis set was carried out to calculate the spin-allowed excitation

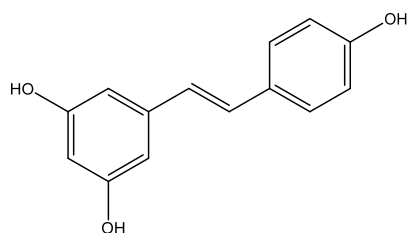
energy and rotatory strength of the lowest 100 excited states. The UV and ECD spectra were generated using the program SpecDis<sup>4</sup> by applying a Gaussian band shape with the width of 0.20 eV, from oscillator strengths and dipole-velocity rotational strengths, respectively. All the calculations were performed with the Gaussian09 program.<sup>5</sup>

### **Biological evaluation**

**Inhibition of NLRP3 inflammasome activation.** THP-1 cells were pretreated with 500 nM PMA for 3 h and then stimulated with 100 ng/mL LPS for 3 h. The cells were further cultured with the test samples for 1 h, followed by challenge incubation with 5 mM ATP. One hour after the challenge, IL-1 $\beta$  levels in the supernatant fraction were analyzed by ELISA. Data are mean  $\pm$  SEM of 3 different experiments.<sup>6</sup>

**Table S1. Small molecules screened in this study.**

Names	Structures
5-azacytidine <sup>7</sup>	
EGCG <sup>8</sup>	
Curcumin <sup>9</sup>	
Thymoquinone <sup>10</sup>	
Procaine <sup>11</sup>	
SAHA <sup>12</sup>	
SBHA <sup>13</sup>	

Resveratrol<sup>14</sup>

EGCG: epigallocatechingallate, SAHA: suberoylanilide hydroxamic acid, SBHA: suberohydroxamic acid.

**Table S2.** <sup>1</sup>H- and <sup>13</sup>C-NMR, and HMBC data for daeschol B in acetone-*d*<sub>6</sub>.

position	$\delta_{\text{H}}$ (multiplicity, <i>J</i> in Hz)	$\delta_{\text{C}}$	HMBC
1		189.5	
2		119.5	
3		163.5	
4	6.07 (d, 2.0)	101.7	C2, C6
5		162.9	
6	6.50 (d, 2.0)	107.2	C4, C2
7		144.5	
8		64.9	
9		128.4	
10	7.48 (d, 8.0)	125.8	C12
11	7.08 (d, 8.0)	114.9	
12		150.9	
13		118.1	
14		159.6	
15	6.89 (d, 8.0)	116.8	C13
16	7.41 (d, 8.0)	128.3	C14
17		137.6	
18		135.9	
19		64.9	
20		141.7	
21	5.68 (d, 8.0)	129.2	C23
22	6.99 (t, 8.0)	139.2	C20
23	6.50 (d, 8.0)	119.4	
24		162.5	
25		117.7	
26		191.0	
27	3.72 (m) 3.20 (m)	37.7	C29, C19
28	3.70 (m)	42.8	
29	3.74 (d, 5.0)	64.3	C27
30		202.7	

**Table S3.** <sup>1</sup>H- and <sup>13</sup>C-NMR data for dalescone A (**13**) in CDCl<sub>3</sub>.

position	$\delta_C$	$\delta_H$ (multiplicity, <i>J</i> in Hz)	position	$\delta_C$	$\delta_H$ (multiplicity, <i>J</i> in Hz)
1	204.5		19	64.2	
2	117.9		20	140.1	
3	157.4		21	118.3	5.88 (d, 8.0)
4	129.6		22	137.3	7.09 (t, 8.0)
5	148.0		23	117.1	6.73 (d, 8.0)
6	116.1	6.83 (s)	24	162.1	
7	136.8		25	117.3	
8	161.8		26	201.0	
9	132.4		27a	42.1	2.86 (dd, 16.5, 7.5)
10	133.4	7.78 (d, 10.0)	27b		3.25 (dd, 16.5, 6.0)
11	133.4	6.79 (d, 10.0)	28	35.9	3.05 (m)
12	188.6		29a	49.7	2.83 (dd, 13.5, 3.0)
13	113.6		29b		3.21 (dd, 13.5, 7.0)
14	159.3		30	74.2	5.11 (m)
15	115.4	6.86 (d, 8.0)	31	71.9	5.11 (m)
16	127.4	7.26 (d, 8.0)	3-OH		12.20 (s)
17	141.5		14-OH		10.69 (s)
18	143.4		24-OH		12.11 (s)

**Table S4.** <sup>1</sup>H- and <sup>13</sup>C-NMR data for dalescone B (**14**) in CDCl<sub>3</sub>.

position	$\delta_C$	$\delta_H$ (multiplicity, <i>J</i> in Hz)	position	$\delta_C$	$\delta_H$ (multiplicity, <i>J</i> in Hz)
1	204.8		19	64.8	
2	118.2		20	140.8	
3	163.7		21	119.0	5.88 (d, 7.7)
4	117.6	6.92 (s)	22	137.9	7.05 (t, 7.7)
5	149.9		23	117.8	6.71 (d, 7.7)
6	122.0	6.98 (s)	24	162.7	
7	137.1		25	117.9	
8	162.5		26	201.7	
9	133.0		27a	42.8	2.86 (dd, 16.5, 7.5)
10	134.2	7.81 (d, 9.8)	27b		3.26 (dd, 16.5, 6.0)
11	134.0	6.79 (d, 9.8)	28	36.9	3.02 (m)
12	189.3		29a	50.4	2.83 (dd, 13.5, 3.0)
13	114.2		29b		3.21 (dd, 13.5, 7.0)
14	160.0		30	64.6	4.73 (s)
15	115.9	6.86 (d, 8.2)	3-OH		12.12 (s)
16	128.0	7.26 (d, 8.2)	14-OH		10.69 (s)
17	142.1		24-OH		12.09 (s)
18	144.2				



**Table S5.**  $^1\text{H}$ - and  $^{13}\text{C}$ -NMR data for dalescone C (**15**) in  $\text{CDCl}_3$ .

position	$\delta_{\text{C}}$	$\delta_{\text{H}}$ (multiplicity, $J$ in Hz)	position	$\delta_{\text{C}}$	$\delta_{\text{H}}$ (multiplicity, $J$ in Hz)
1	205.2		19	64.6	
2	119.1		20	140.8	
3	163.4		21	119.0	5.84 (d, 8.0)
4	120.8	6.94 (d, 8.0)	22	137.9	7.03 (t, 8.0)
5	136.1	7.46 (t, 8.0)	23	117.7	6.70 (d, 8.0)
6	124.8	6.97 (d, 8.0)	24	162.7	
7	136.9		25	117.8	
8	163.1		26	201.7	
9	142.1		27a	43.0	2.88 (dd, 16.6, 7.2)
10	130.2	7.87 (s)	27b		3.28 (dd, 16.6, 6.2)
11	144.3		28	37.2	2.97 (m)
12	189.2		29a	50.6	2.83 (dd, 13.3, 2.8)
13	113.9		29b		3.25 (dd, 13.3, 6.9)
14	160.1		30	62.5	4.77 (dd, 23.5, 14.8)
15	115.8	6.85 (d, 8.4)	3-OH		12.00 (s)
16	128.1	7.27 (d, 8.4)	14-OH		10.66 (s)
17	132.2		24-OH		12.12 (s)
18	143.4				

**Table S6.**  $^1\text{H}$ - and  $^{13}\text{C}$ -NMR data for dalescone D (**16**) in  $\text{CDCl}_3$ .

position	$\delta_{\text{C}}$	$\delta_{\text{H}}$ (multiplicity, $J$ in Hz)	position	$\delta_{\text{C}}$	$\delta_{\text{H}}$ (multiplicity, $J$ in Hz)
1	204.5		19	63.9	
2	118.8		20	140.2	
3	162.7		21	118.4	5.84 (d, 8.0)
4	120.1	6.94 (d, 8.0)	22	137.2	7.03 (t, 8.0)
5	135.5	7.46 (t, 8.0)	23	117.0	6.70 (d, 8.0)
6	124.1	6.97 (d, 8.0)	24	162.0	
7	136.3		25	117.3	
8	162.4		26	201.0	
9	141.4		27a	42.4	2.88 (dd, 16.6, 7.2)
10	128.1	7.87 (s)	27b		3.28 (dd, 16.6, 6.2)
11	146.9		28	36.6	2.97 (m)
12	188.5		29a	49.9	2.83 (dd, 13.3, 2.8)
13	113.5		29b		3.25 (dd, 13.3, 6.9)
14	159.6		30	67.1	5.12 (d, 6.4)
15	115.2	6.85 (d, 8.4)	31	23.1	1.65 (d, 6.4)
16	127.3	7.27 (d, 8.4)	3-OH		12.00 (s)
17	131.6		14-OH		10.76 (s)
18	143.4		24-OH		12.12 (s)

**Table S7.**  $^1\text{H}$ -NMR data for dalescone E (**17**) in  $\text{DMSO}-d_6$ .

position	$\delta_{\text{H}}$ (multiplicity, $J$ in Hz)	position	$\delta_{\text{H}}$ (multiplicity, $J$ in Hz)
4	6.20 (d, 2.4)	28	2.90 (m)
6	6.54 (d, 2.4)	29a	2.62 (dd, 13.3, 2.8)
10	8.04 (s)	29b	3.24 (dd, 13.3, 6.9)
15	6.82 (d, 8.0)	30	4.96 (m)
16	7.66 (d, 8.0)	31	1.644 (d, 6.4)
21	5.88 (d, 8.0)	3-OH	12.18 (s)
22	7.14 (t, 8.0)	5-OH	11.04 (s)
23	6.67 (d, 8.0)	11-OH	5.39 (d, 4.4)
27a	2.81 (dd, 16.6, 3.6)	14-OH	10.79 (s)
27b	3.49 (dd, 16.6, 6.8)	24-OH	12.43 (s)

**Table S8.**  $^1\text{H}$ -NMR data for dalescone F (**18**) in  $\text{CDCl}_3$ .

position	$\delta_{\text{H}}$ (multiplicity, $J$ in Hz)	position	$\delta_{\text{H}}$ (multiplicity, $J$ in Hz)
4	6.33 (d, 2.0)	27b	3.20 (dd, 16.6, 6.2)
6	6.47 (d, 2.0)	28	3.05 (m)
10	7.83 (s)	29a	2.75 (dd, 13.3, 2.8)
15	6.86 (d, 8.4)	29b	3.08 (dd, 13.3, 6.9)
16	7.26 (d, 8.4)	30	4.77 (dd, 35.5, 14.2)
21	5.89 (d, 8.0)	3-OH	12.55 (s)
22	7.08 (t, 8.0)	6-OH	6.24 (s)
23	6.73 (d, 8.0)	14-OH	10.60 (s)
27a	2.85 (dd, 16.6, 7.2)	24-OH	12.09 (s)

**Table S9.**  $^1\text{H}$ -NMR data for dalescone G (**19**) in  $\text{CDCl}_3$ .

position	$\delta_{\text{H}}$ (multiplicity, $J$ in Hz)	position	$\delta_{\text{H}}$ (multiplicity, $J$ in Hz)
6	6.84 (s)	28	3.03 (m)
10	7.74 (d, 10.0)	29a	2.83 (dd, 13.5, 3.0)
11	6.79 (d, 10.0)	29b	3.21 (dd, 13.5, 7.0)
15	6.87 (d, 8.0)	30	6.16 (d, 1.8)
16	7.26 (d, 8.0)	31a	4.98 (d, 14.3)
21	5.87 (d, 8.0)	31b	5.23 (dd, 14.3, 1.8)
22	7.07 (t, 8.0)	3-OH	12.39 (s)
23	6.73 (d, 8.0)	14-OH	10.66 (s)
27a	2.86 (dd, 16.5, 7.5)	24-OH	12.10 (s)
27b	3.25 (dd, 16.5, 6.0)	30-OCH <sub>3</sub>	3.51 (s)

**Table S10.** Inhibitory assay against IL-1 $\beta$  production in THP-1 cells with LPS+ATP induced NLRP3 inflammasome activation (IC<sub>50</sub> in  $\mu$ M).

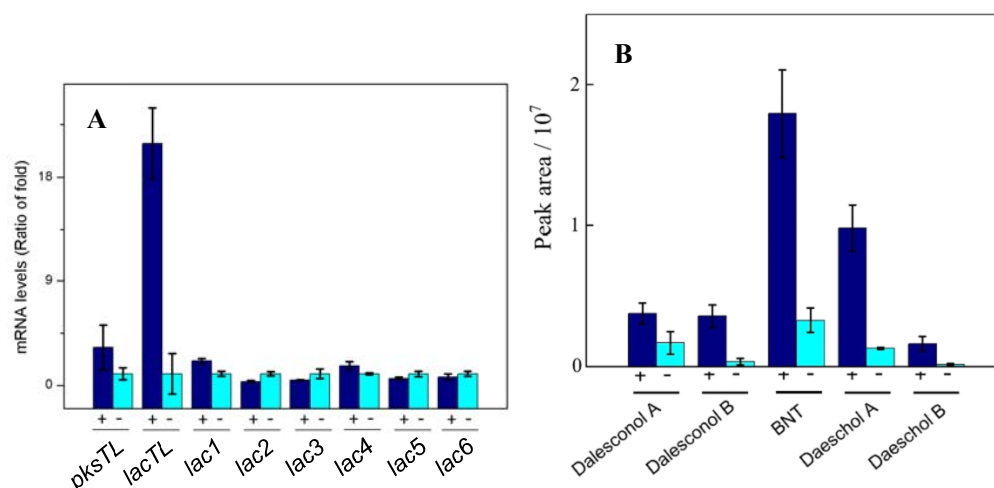
Cell line	compounds									
	(+)- <b>13</b>	(-)- <b>13</b>	(+)- <b>14</b>	(-)- <b>14</b>	(+)- <b>15</b>	(-)- <b>15</b>	(+)- <b>16a</b>	(-)- <b>16a</b>	(+)- <b>16b</b>	(-)- <b>16b</b>
THP-1	5.2	>10	9.4	>10	13.0	>10	4.9	3.9	>10	>10

Cell line	compounds									
	(+)-daeschol B	(-)-daeschol B	(+)- <b>17</b>	(-)- <b>17</b>	(+)- <b>18</b>	(-)- <b>18</b>	(+)- <b>19a</b>	(-)- <b>19a</b>	(+)- <b>19b</b>	(-)- <b>19b</b>
THP-1	>10	>10	>10	>10	>10	>10	5.4	5.7	5.6	5.7

## References

- [1] Y. L. Zhang, H. M. Ge, W. Zhao, H. Dong, Q. Xu, S. H. Li, J. Li, J. Zhang, Y. C. Song, R. X. Tan, *Angew. Chem. Int. Ed.* **2008**, *47*, 5823–5826.
- [2] Y. L. Zhang, J. Zhang, N. Jiang, Y. H. Lu, L. Wang, S. H. Xu, W. Wang, G. F. Zhang, Q. Xu, H. M. Ge, J. Ma, Y. C. Song, R. X. Tan, *J. Am. Chem. Soc.* **2011**, *133*, 5931–5940.
- [3] W. Fang, S. Ji, N. Jiang, W. Wang, G. Y. Zhao, S. Zhang, H. M. Ge, Q. Xu, A. H. Zhang, Y. L. Zhang, Y. C. Song, J. Zhang, R. X. Tan, *Nat. Commun.* **2012**, *3*, 1039.
- [4] S. K. Han, P. Bilski, B. Karriker, R. H. Sik, C. F. Chignell, *Environ. Sci. Technol.* **2008**, *42*, 166–172.
- [5] M. J. Frisch, G. W. Trucks, H. B. Schlegel, G. E. Scuseria, M. A. Robb, J. R. Cheeseman, G. Scalmani, V. Barone, B. Mennucci, G. A. Petersson, H. Nakatsuji, M. Caricato, X. Li, H. P. Hratchian, A. F. Izmaylov, J. Bloino, G. Zheng, J. L. Sonnenberg, M. Hada, M. Ehara, K. Toyota, R. Fukuda, J. Hasegawa, M. Ishida, T. Nakajima, Y. Honda, O. Kitao, H. Nakai, T. Vreven, J. A. Montgomery, Jr., J. E. Peralta, F. Ogliaro, M. Bearpark, J. J. Heyd, E. Brothers, K. N. Kudin, V. N. Staroverov, R. Kobayashi, J. Normand, K. Raghavachari, A. Rendell, J. C. Burant, S. S. Iyengar, J. Tomasi, M. Cossi, N. Rega, J. M. Millam, M. Klene, J. E. Knox, J. B. Cross, V. Bakken, C. Adamo, J. Jaramillo, R. Gomperts, R. E. Stratmann, O. Yazyev, A. J. Austin, R. Cammi, C. Pomelli, J. W. Ochterski, R. L. Martin, K. Morokuma, V. G. Zakrzewski, G. A. Voth, P. Salvador, J. J. Dannenberg, S. Dapprich, A. D. Daniels, Ö. Farkas, J. B. Foresman, J. V. Ortiz, J. Cioslowski, and D. J. Fox, Gaussian 09, Revision A.1, Gaussian, Inc., Wallingford CT, **2009**.
- [6] W. Guo, Y. Sun, W. Liu, X. Wu, L. Guo, P. Cai, X. Wu, X. Wu, Y. Shen, Y. Shu, Y. Gu, Q. Xu, *Autophagy* **2014**, *10*, 972–985.
- [7] Christman, J. K. 5-Azacytidine and 5-aza-2'-deoxycytidine as inhibitors of DNA methylation: mechanistic studies and their implications for cancer therapy. *Oncogene* **21**, 5483–5495 (2002).
- [8] J. B. Berletch *et al.*, Epigenetic and genetic mechanisms contribute to telomerase inhibition by EGCG. *J. Cell. Biochem.* **103**, 509–519 (2008).
- [9] S. Reuter, S. C. Gupta, B. Park, A. Goel, B. B. Aggarwal, Epigenetic changes induced by curcumin and other natural compounds. *Genes Nutr.* **6**, 93–108 (2011).
- [10] E. S. A. Arafa *et al.*, Thymoquinone up-regulates PTEN expression and induces apoptosis in doxorubicin-resistant human breast cancer cells. *Mutat. Res- Fund. Mol. M.* **706**, 28–35 (2011).
- [11] A. Villar-Garea, M. F. Fraga, J. Espada, M. Esteller, Procaine is a DNA-demethylating agent with growth-inhibitory effects in human cancer cells. *Cancer Res.* **63**, 4984–4989 (2003).
- [12] W. K. Kelly, P. A. Marks, Drug insight: histone deacetylase inhibitors—development of the new targeted anticancer agent suberoylanilide hydroxamic acid. *Nat. Clin. Pract. Oncol.* **2**, 150–157 (2005).
- [13] F. Vandermeers *et al.*, The role of epigenetics in malignant pleural mesothelioma. *Lung Cancer-J Iaslc.* **81**, 311–318 (2013).
- [14] A. J. Papoutsis, S. D. Lamore, G. T. Wondrak, O. I. Selmin, D. F. Romagnolo, Resveratrol prevents epigenetic silencing of BRCA-1 by the aromatic hydrocarbon receptor in human breast cancer cells. *J. Nutr.* **140**, 1607–1614 (2010).



**Figure S1.** A), qRT-PCR comparison of the transcriptional levels of genes that encoding laccases (*lacTL*, *lac1-6*) and polyketide synthase (*pksTL*) of *D. eschscholzii* cultured with (+) or without (-) procaine. B), LC-MS based abundance comparisons of naphthol dimers (1,1'-binaphthalene-4,4',5,5'-tetrol, BNT) and and trimers (daeschol A and its decarboxylative product—dalesconol A).

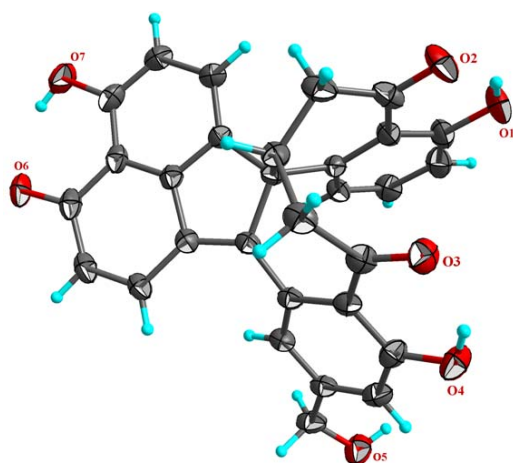


**Figure S2.** X-ray crystal structure of dalescone B (14).

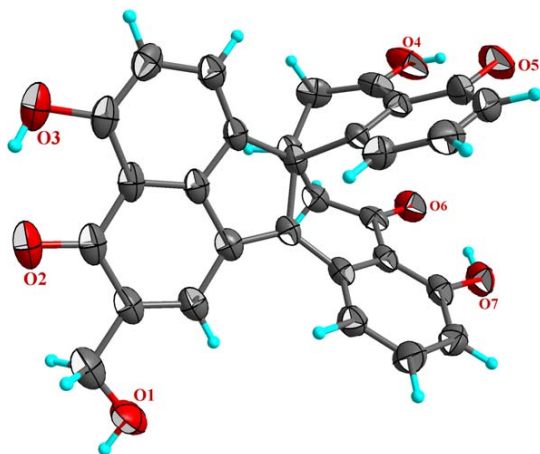


**Figure S3.** X-ray crystal structure of dalescone C (**15**).

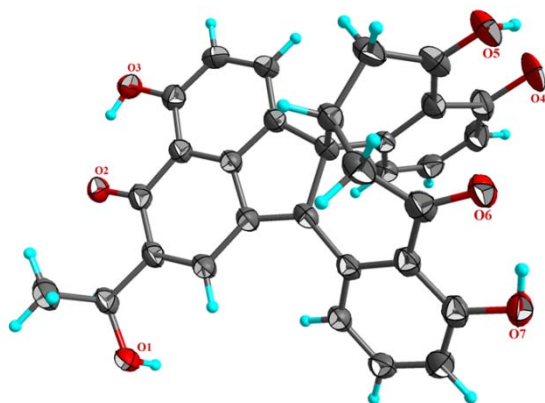


**Figure S4.** X-ray crystal structure of dalescone D (**16a**).

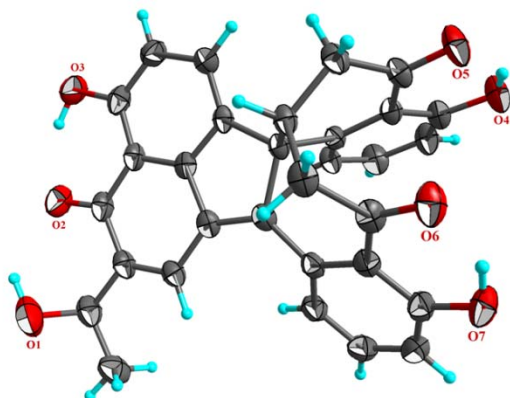


**Figure S5.** X-ray crystal structure of dalescone D (**16b**).

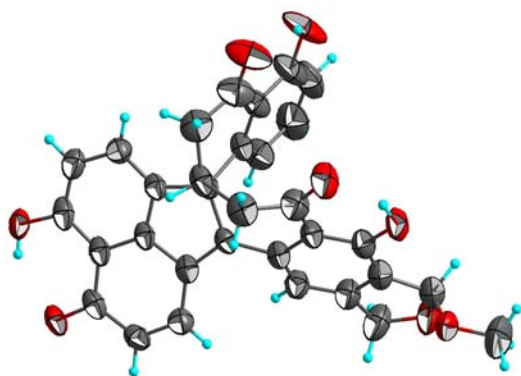


**Figure S6.** X-ray crystal structure of dalescone G (**19a**).

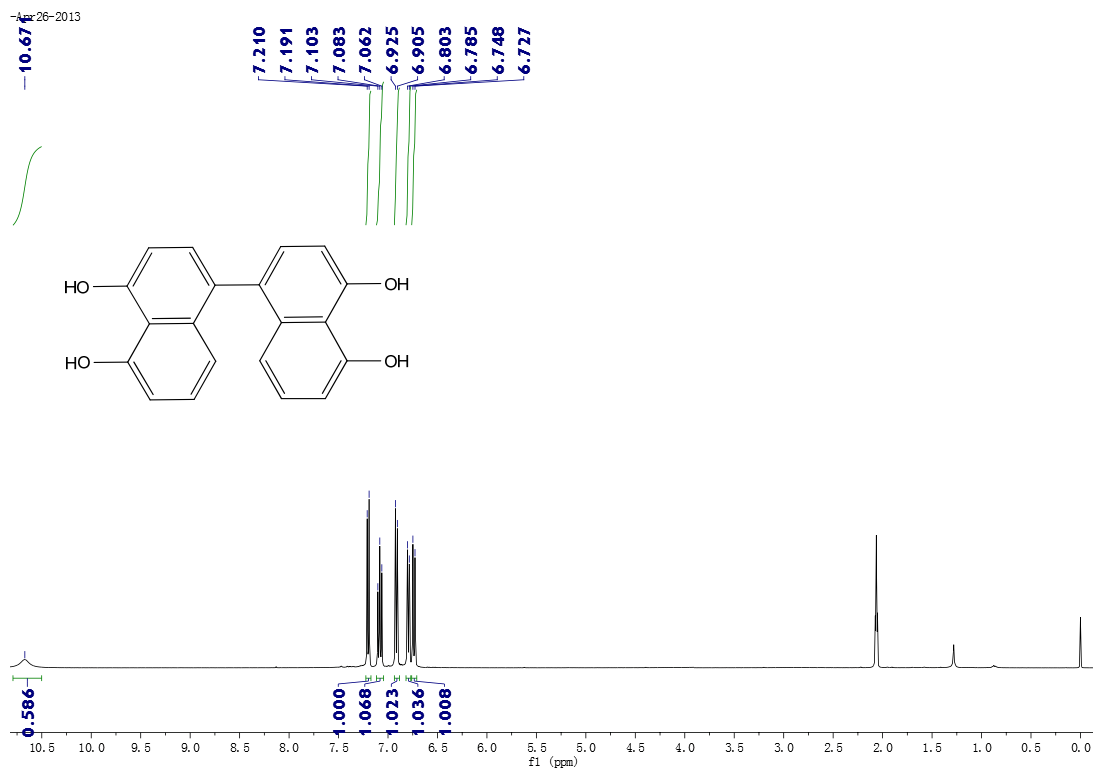


**Figure S7.**  $^1\text{H}$ -NMR spectrum of BNT (400 MHz, acetone- $d_6$ ).

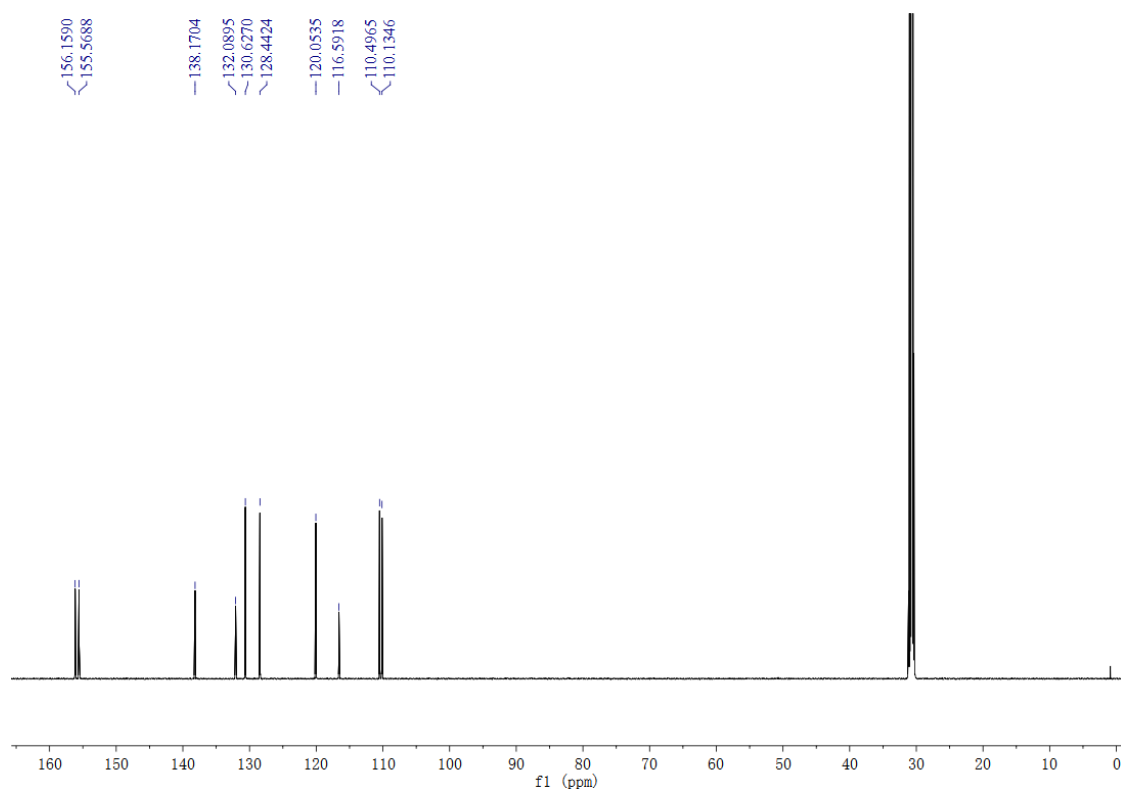


**Figure S8.**  $^{13}\text{C}$ -NMR spectrum of BNT (150 MHz, acetone- $d_6$ ).

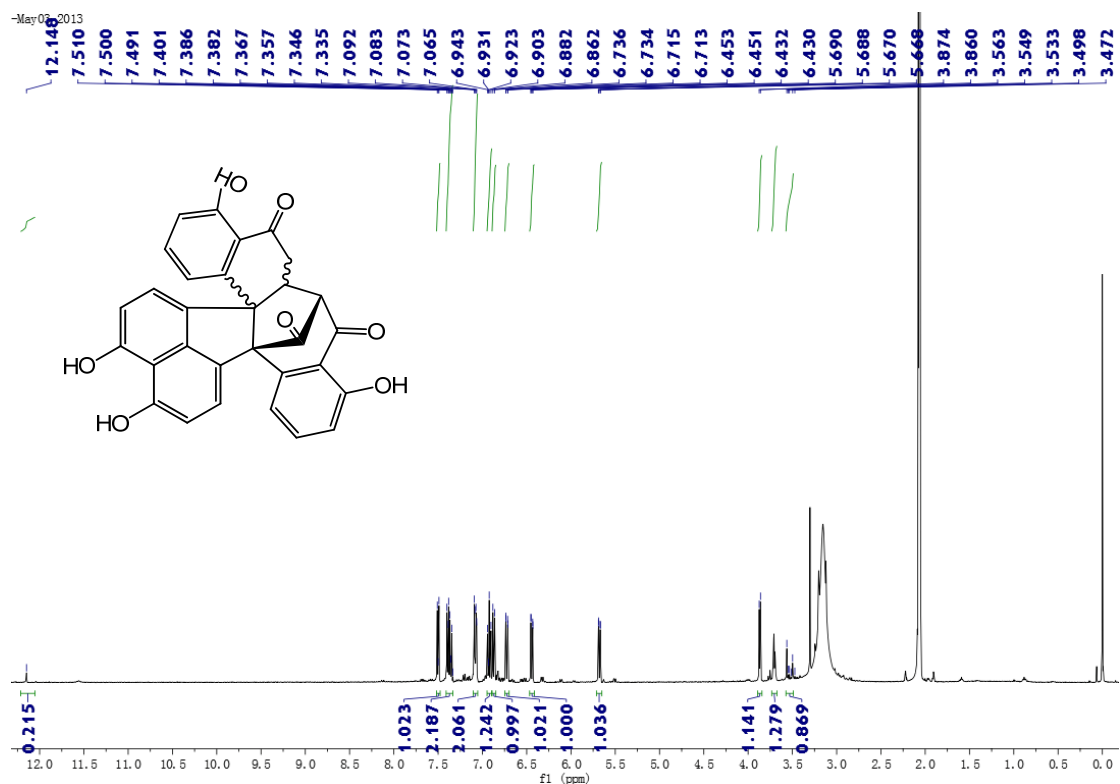


**Figure S9.**  $^1\text{H}$ -NMR spectrum of daeschol A (400 MHz, acetone- $d_6$ ).

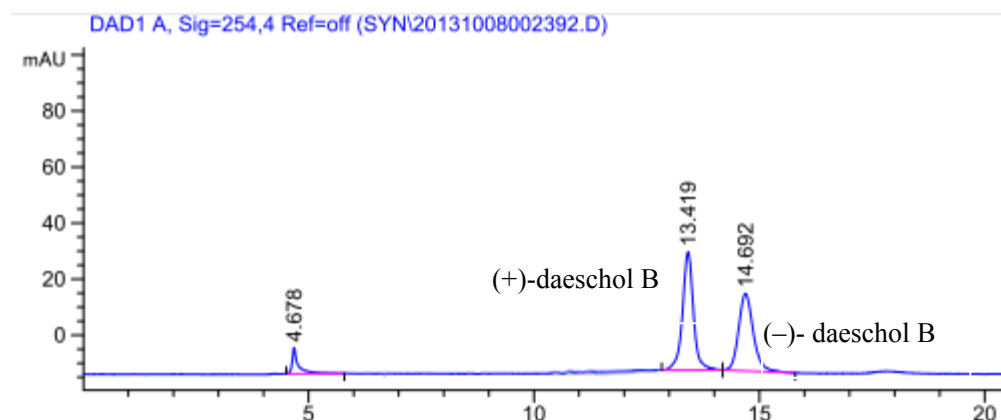


**Figure S10.** Chiral HPLC separation of daeschol B.

<Column Performance Report>

Column: CHIRALPAK<sup>®</sup> IA<sup>™</sup>, 0.50 cm ID. × 25 cm L, 5  $\mu\text{m}$

Mobile Phase: DCM/MeOH = 15/85 (v/v)

Peak No.	Time	Area	Area %
1	13.419	712.0	47.0608
2	14.692	623.1	41.1274



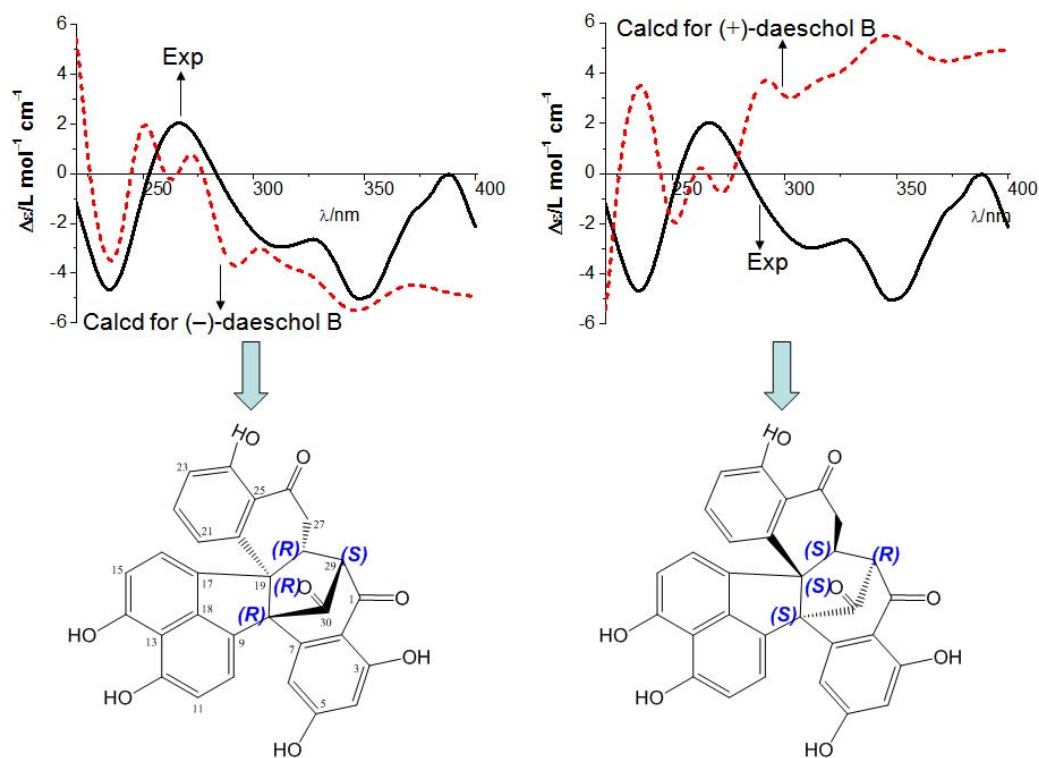


**Figure S11.** Absolute configurations of (+)- and (-)-daeschol B by comparing the experimental and calculated ECD spectra.

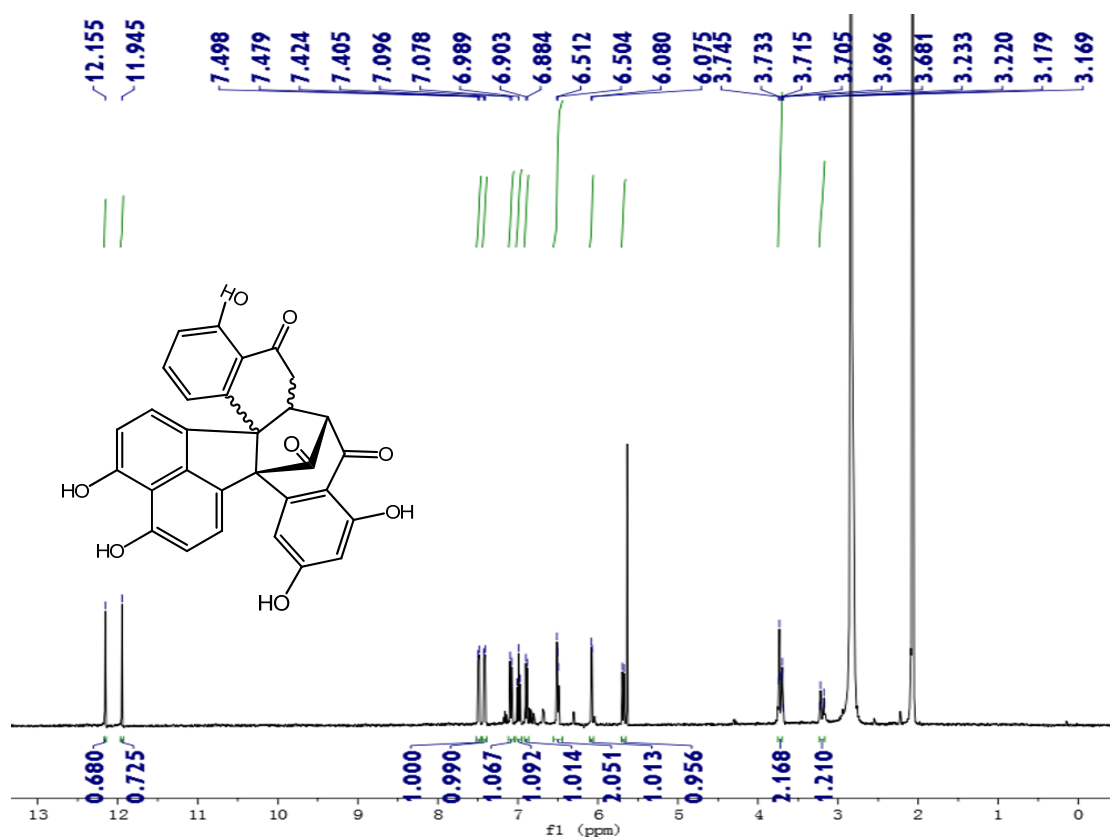


**Figure S12.**  $^1\text{H}$ -NMR spectrum of daeschol B (400 MHz, acetone- $d_6$ ).

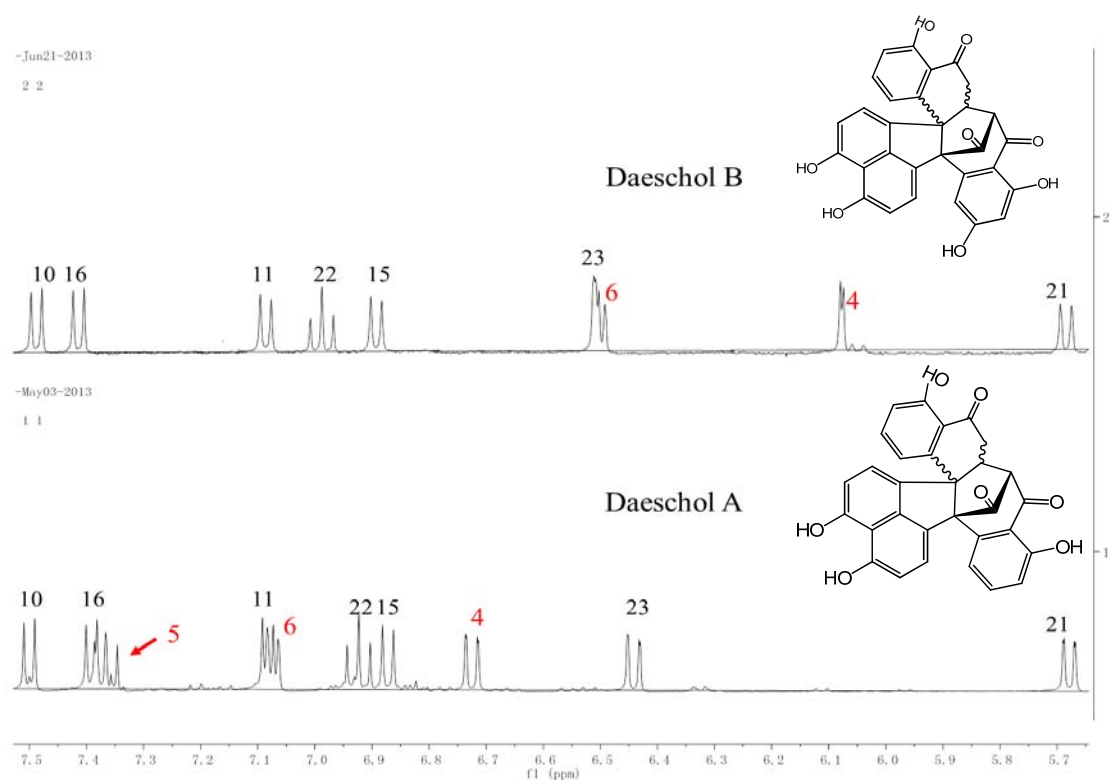


**Figure S13.** Comparison of  $^1\text{H}$ -NMR spectra of daeschol A and B (400 MHz, acetone- $d_6$ ).

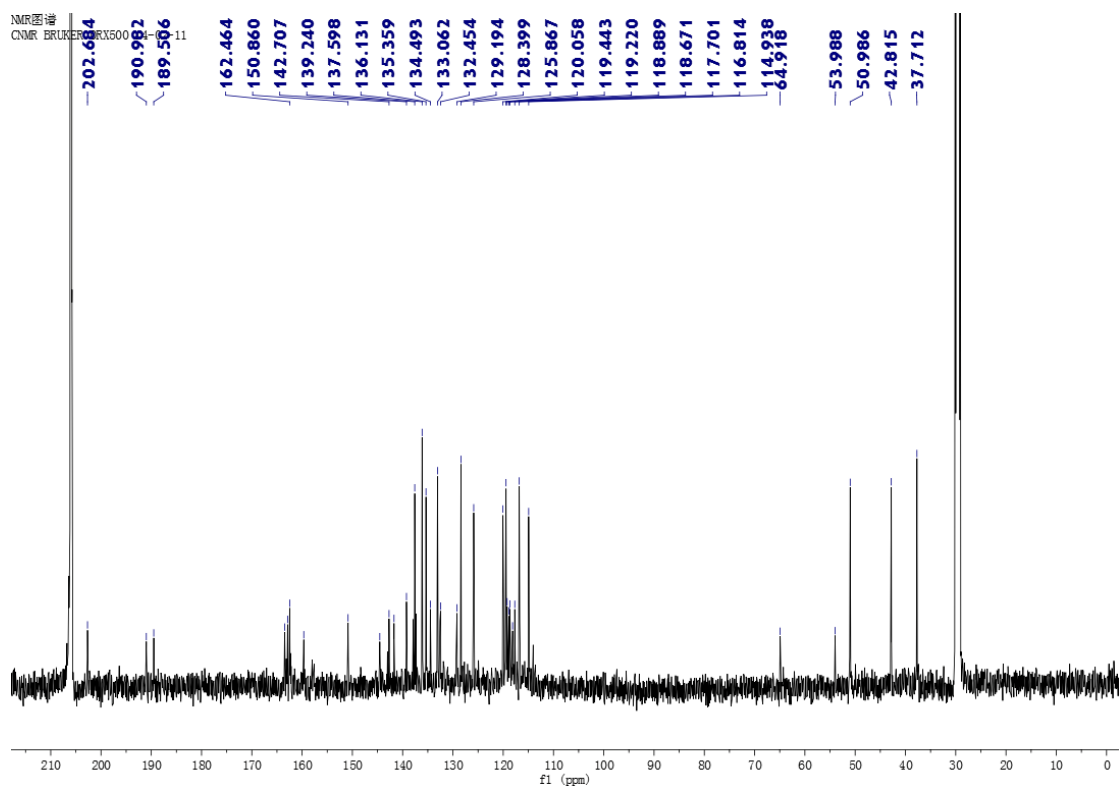


**Figure S14.**  $^{13}\text{C}$ -NMR spectrum of daeschol B (125 MHz, acetone- $d_6$ ).

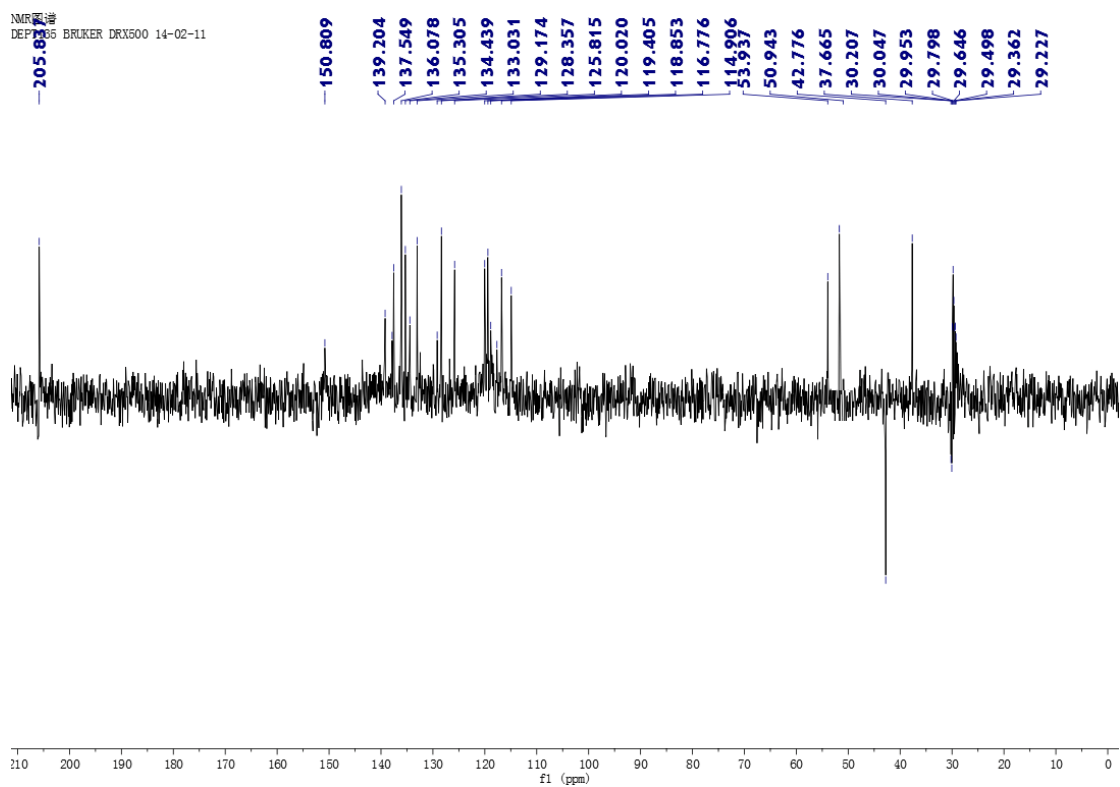


**Figure S15.** DEPT spectrum of daeschol B (acetone- $d_6$ ).

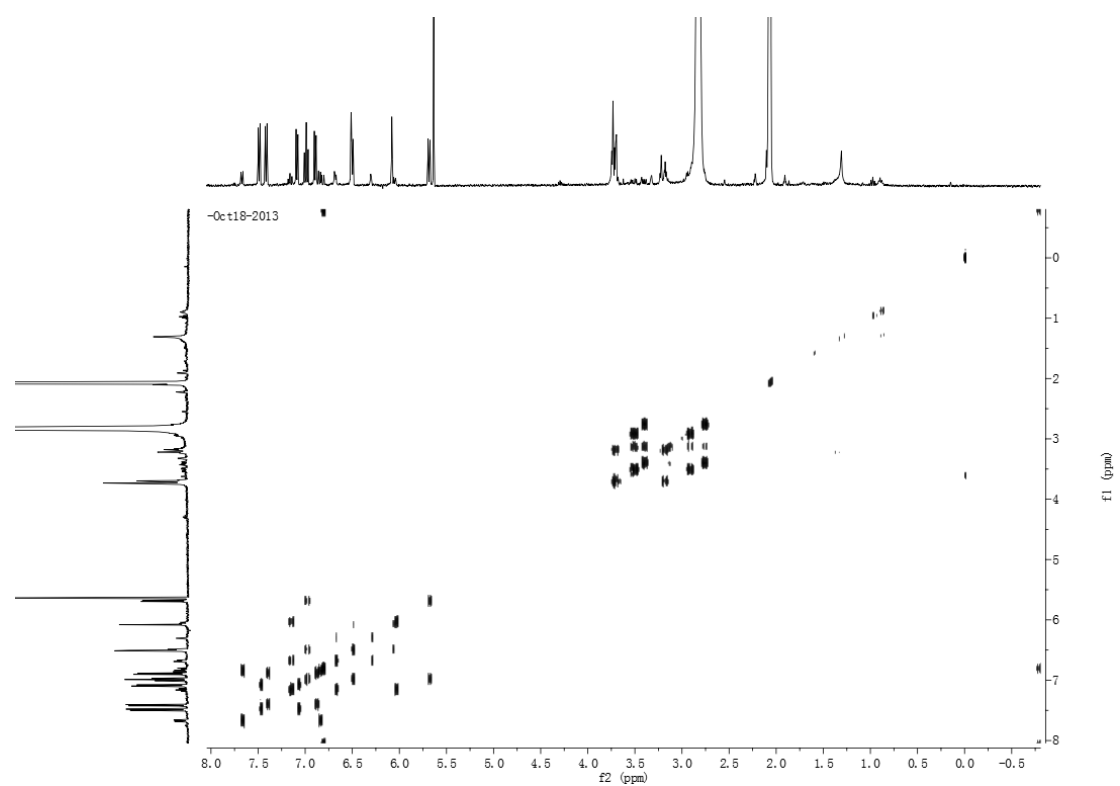


**Figure S16.**  $^1\text{H}$ - $^1\text{H}$  COSY spectrum of daeschol B (acetone- $d_6$ ).

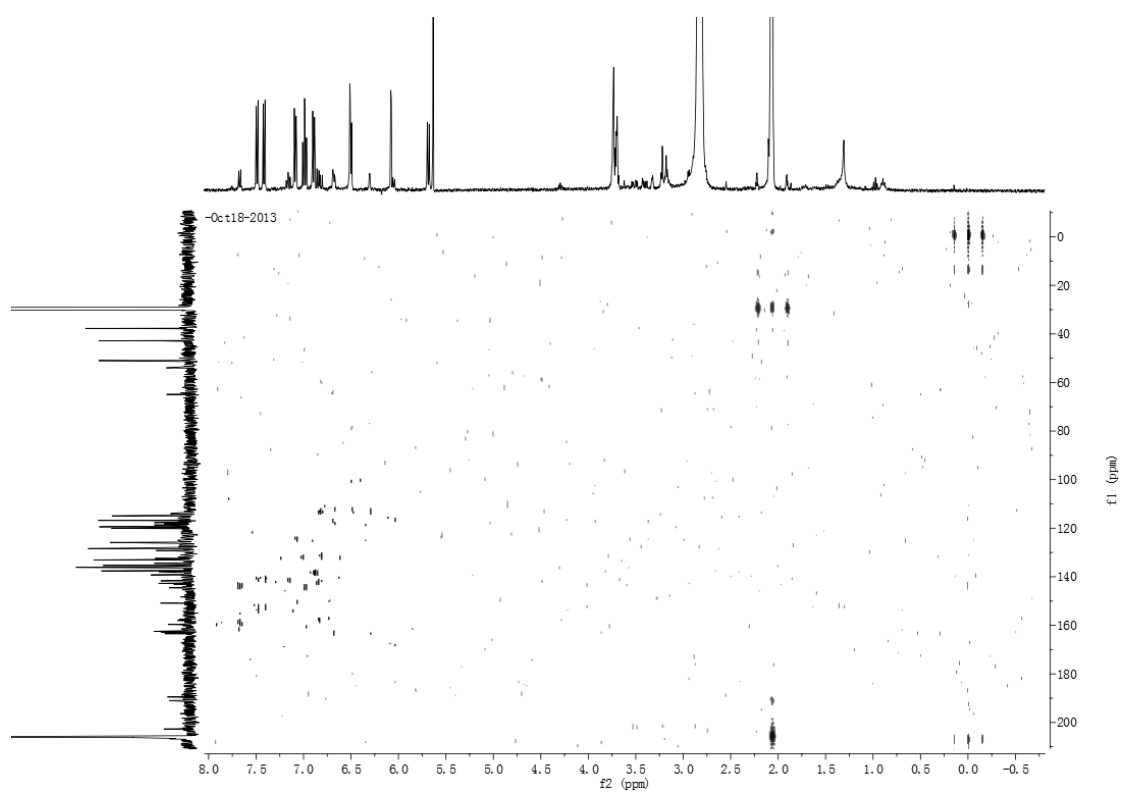


**Figure S17.** HSQC spectrum of daeschol B (acetone- $d_6$ ).

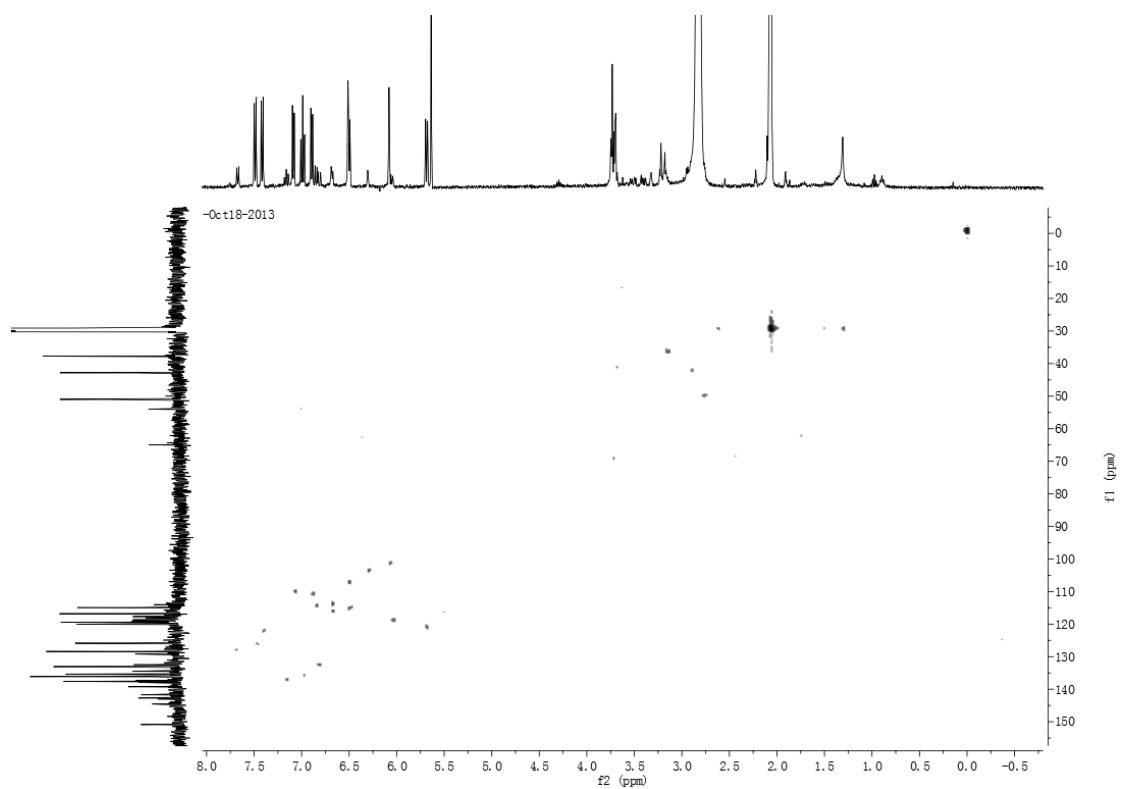


**Figure S18.** HMBC spectrum of daeschol B (acetone- $d_6$ ).

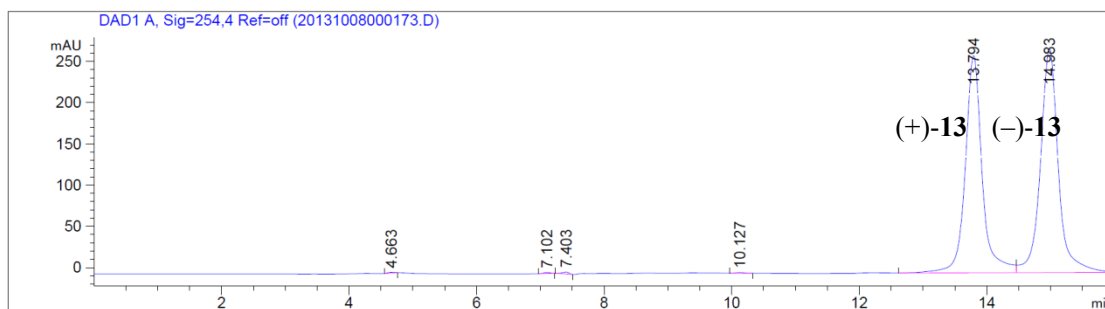


**Figure S19.** Chiral HPLC separation of dalescone A (**13**).

<Column Performance Report>

Column: CHIRALPAK® IA™, 0.50 cm ID. × 25 cm L, 5 μm

Mobile Phase: DCM/MeOH = 30/70 (v/v)

Peak No.	Time	Area	Area %
1	13.794	4868	47.7278
2	14.983	5289	51.8480

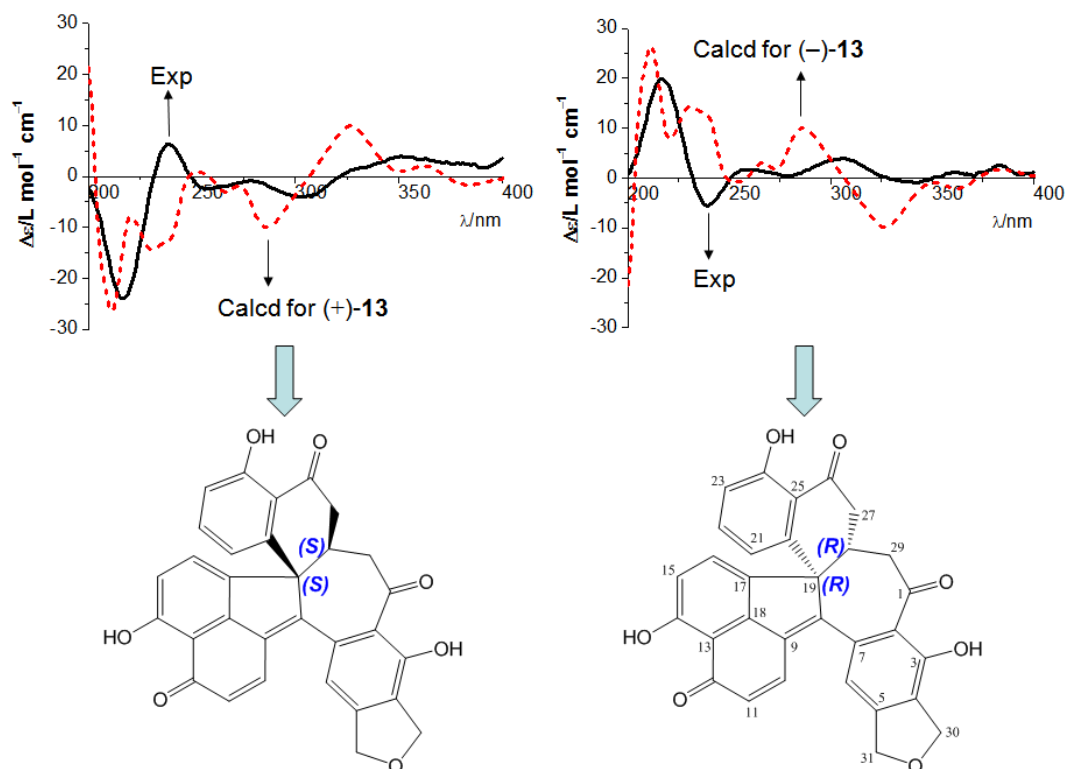


**Figure S20.** Absolute configurations of (+)- and (-)-**13** by comparing the experimental and calculated ECD spectra.

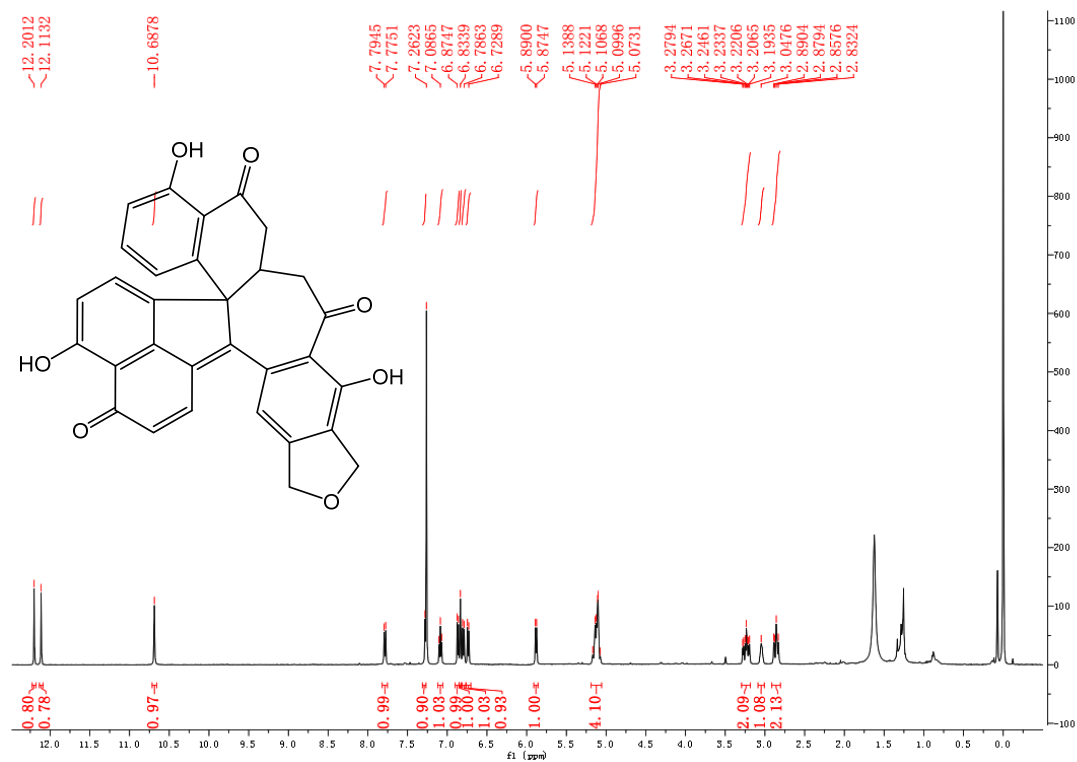


**Figure S21.**  $^1\text{H}$ -NMR spectrum of dalescone A (**13**, 500 MHz,  $\text{CDCl}_3$ ).

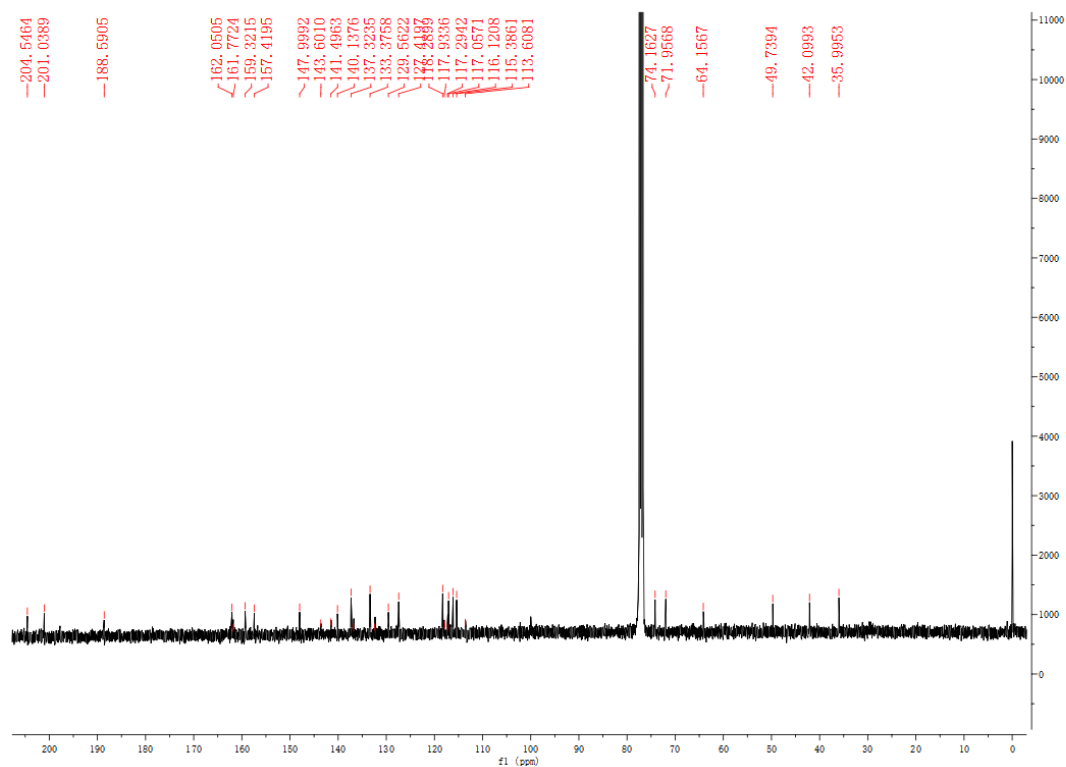


**Figure S22.**  $^{13}\text{C}$ -NMR spectrum of dalescone A (**13**, 125 MHz,  $\text{CDCl}_3$ ).

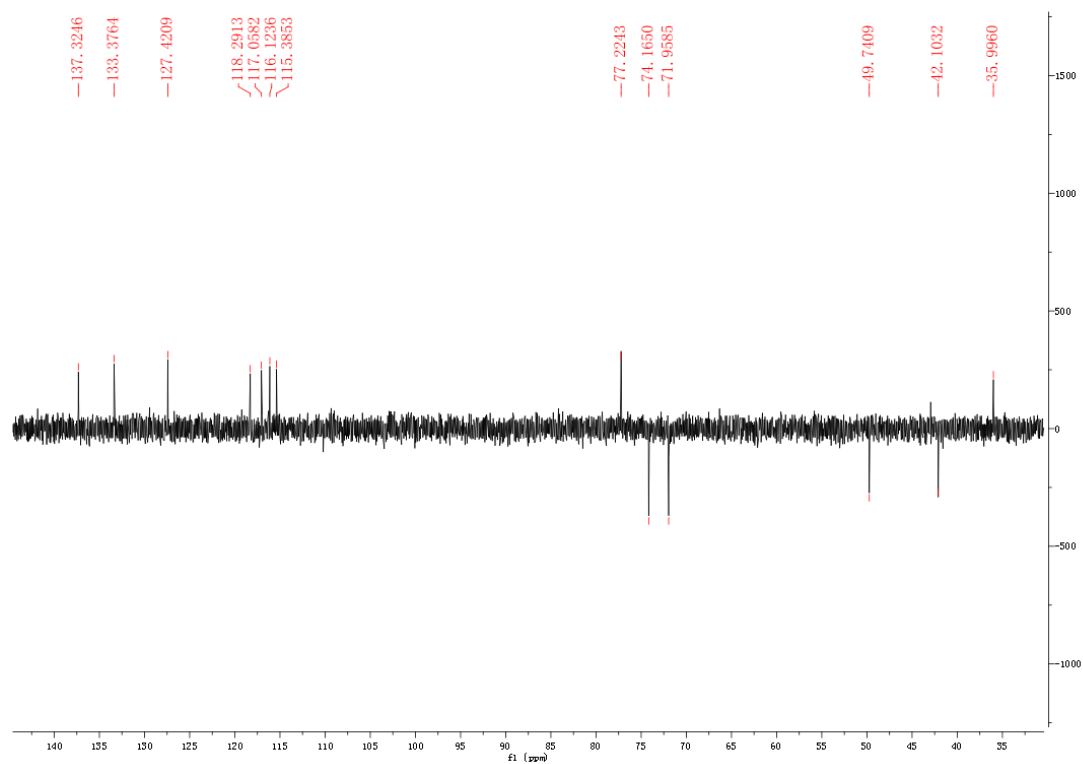


**Figure S23.** DEPT spectrum of dalescone A (**13**,  $\text{CDCl}_3$ ).

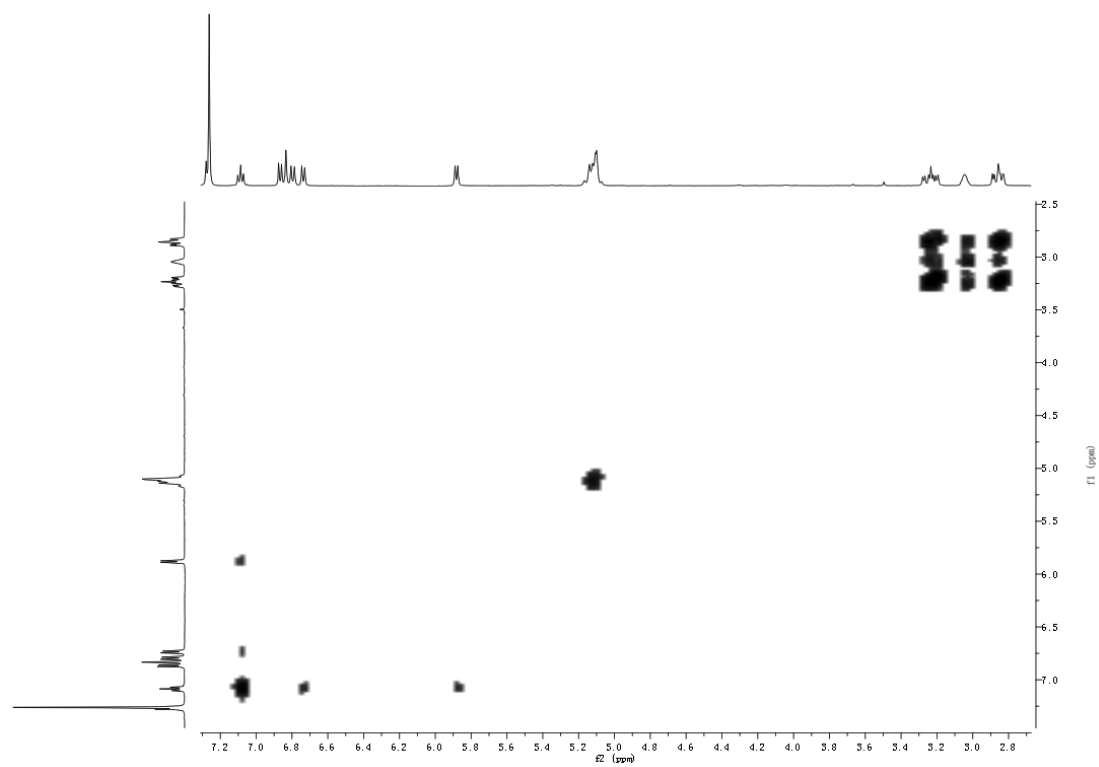


**Figure S24.**  $^1\text{H}$ - $^1\text{H}$  COSY spectrum of dalescone A (**13**,  $\text{CDCl}_3$ ).

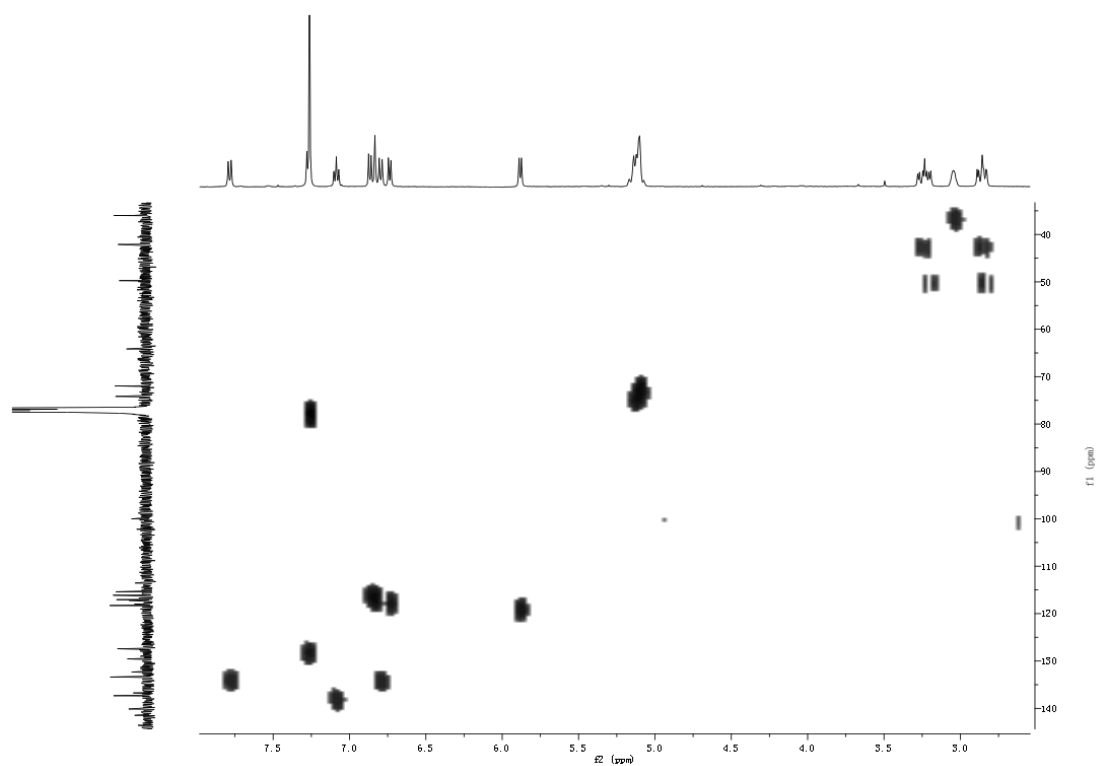


**Figure S25.** HSQC spectrum of dalescone A (**13**, CDCl<sub>3</sub>).

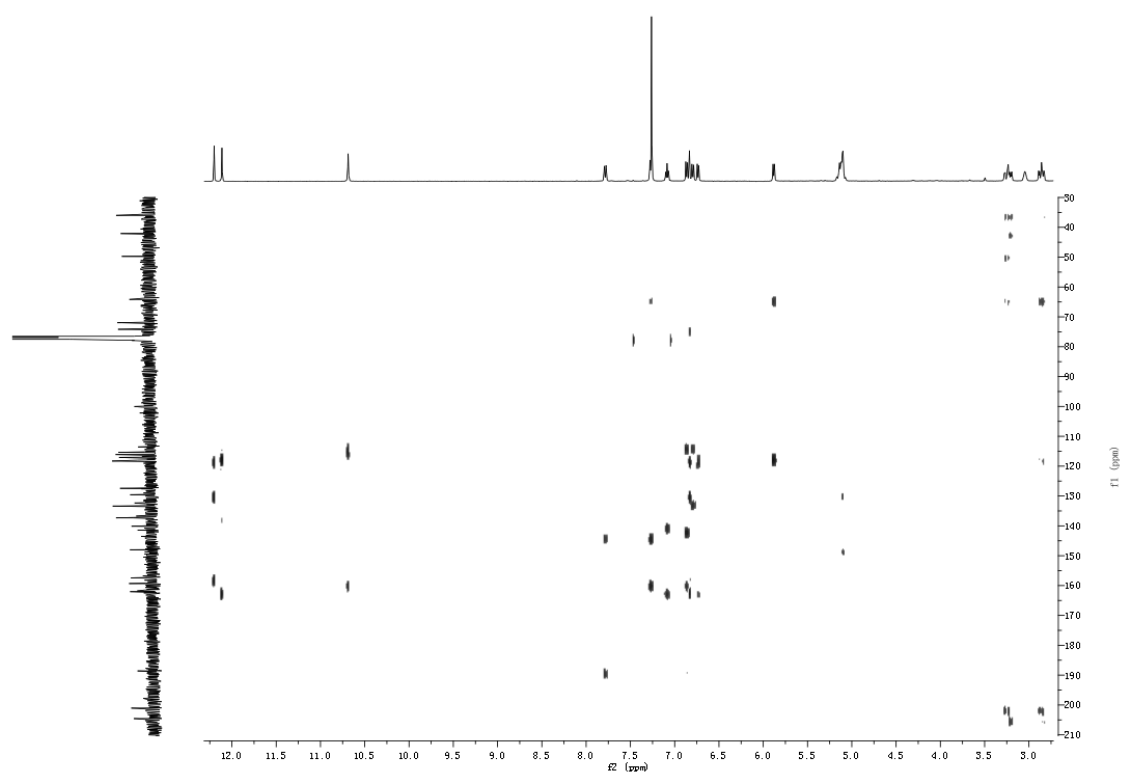


**Figure S26.** HMBC spectrum of dalescone A (**13**, CDCl<sub>3</sub>).



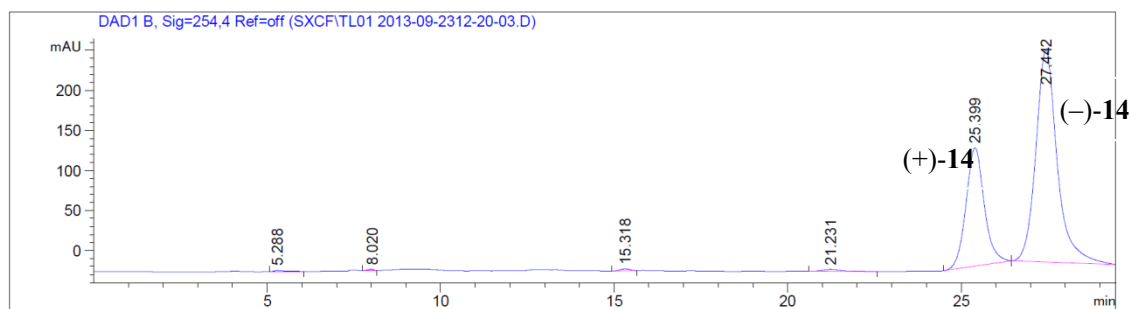


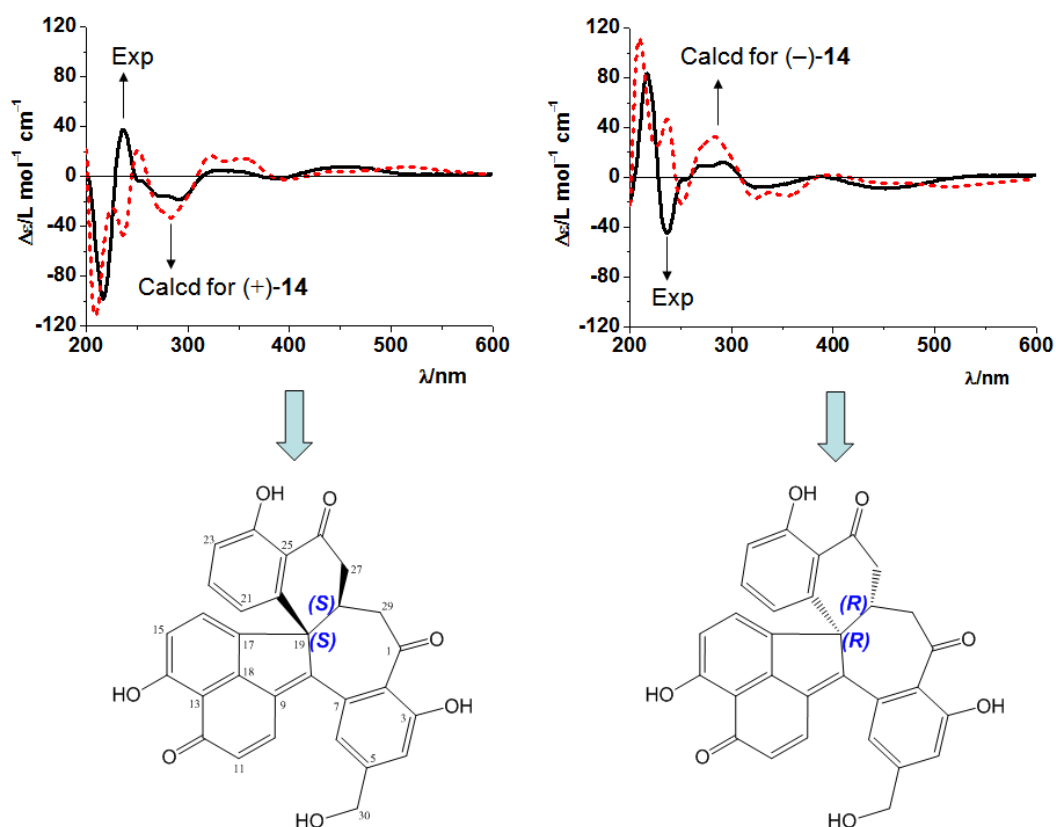
**Figure S27.** Chiral HPLC separation of dalescone B (**14**).

<Column Performance Report>

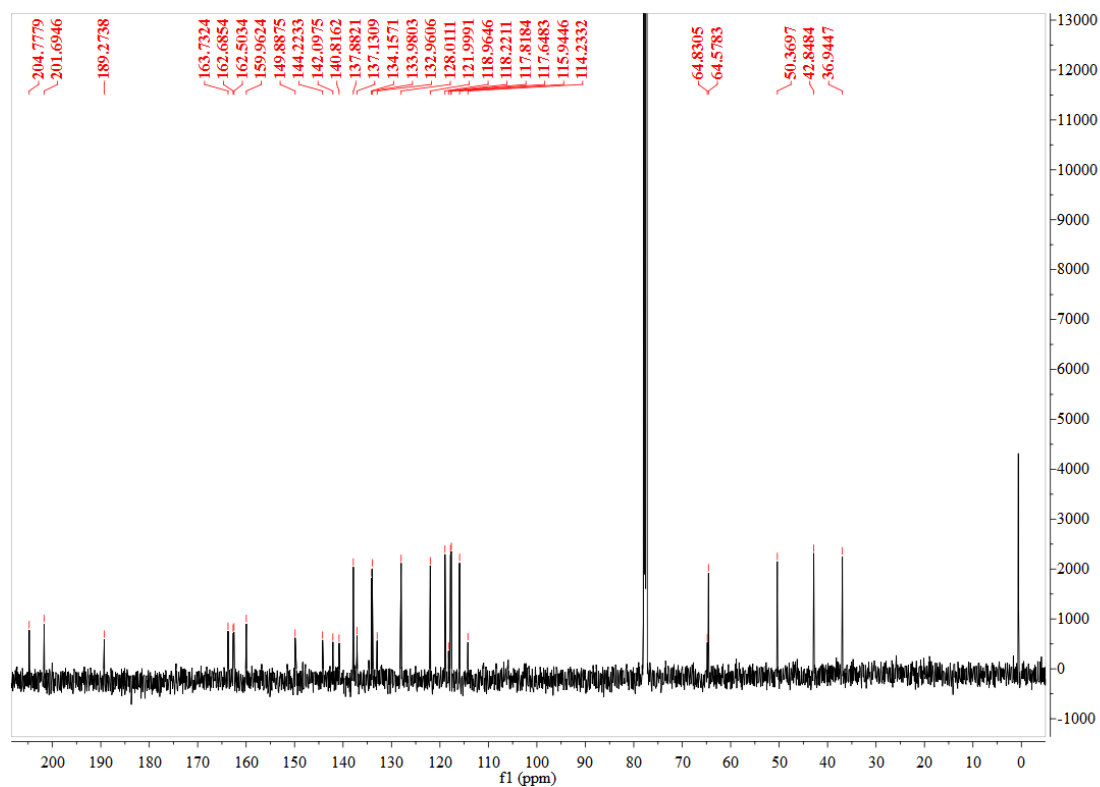
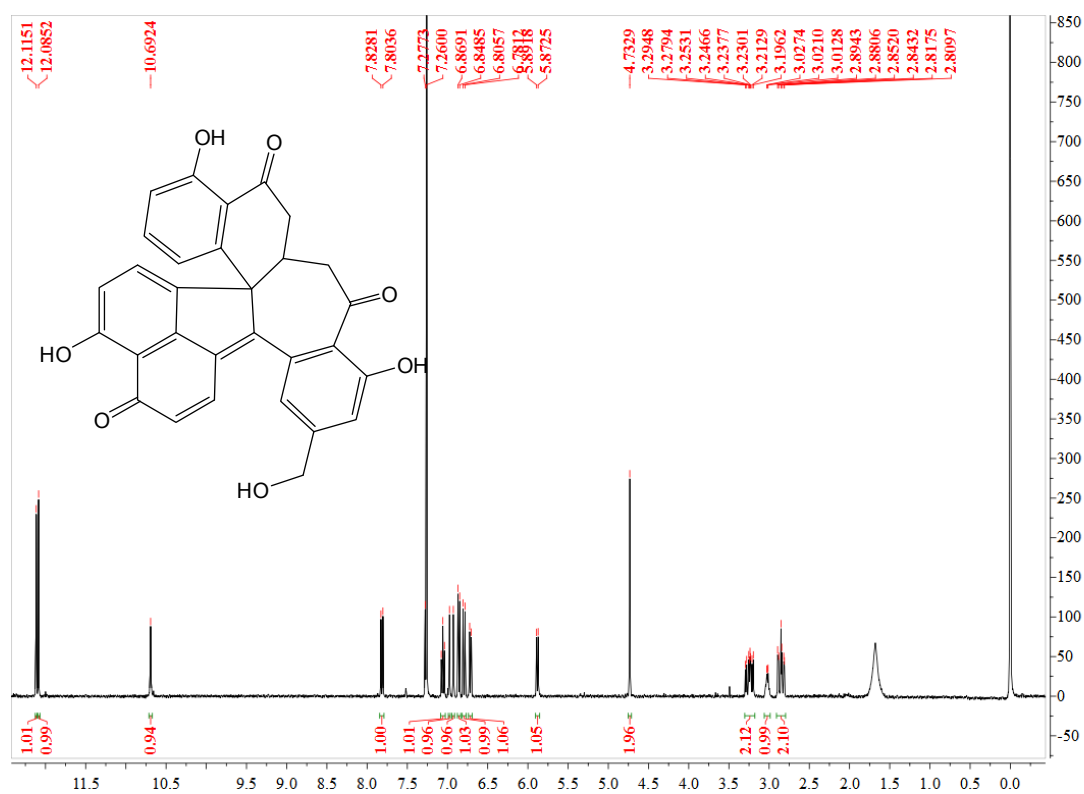
Column: CHIRALPAK® IA™, 0.50 cm ID. × 25 cm L, 5 μm

Mobile Phase: Hex/EtOH = 50/50 (v/v)

Peak No.	Time	Area	Area %
1	25.399	5417	31.8411
2	27.442	11415	67.0921



**Figure S28.** Absolute configurations of (+)- and (-)-**14** by comparing the experimental and calculated ECD spectra.



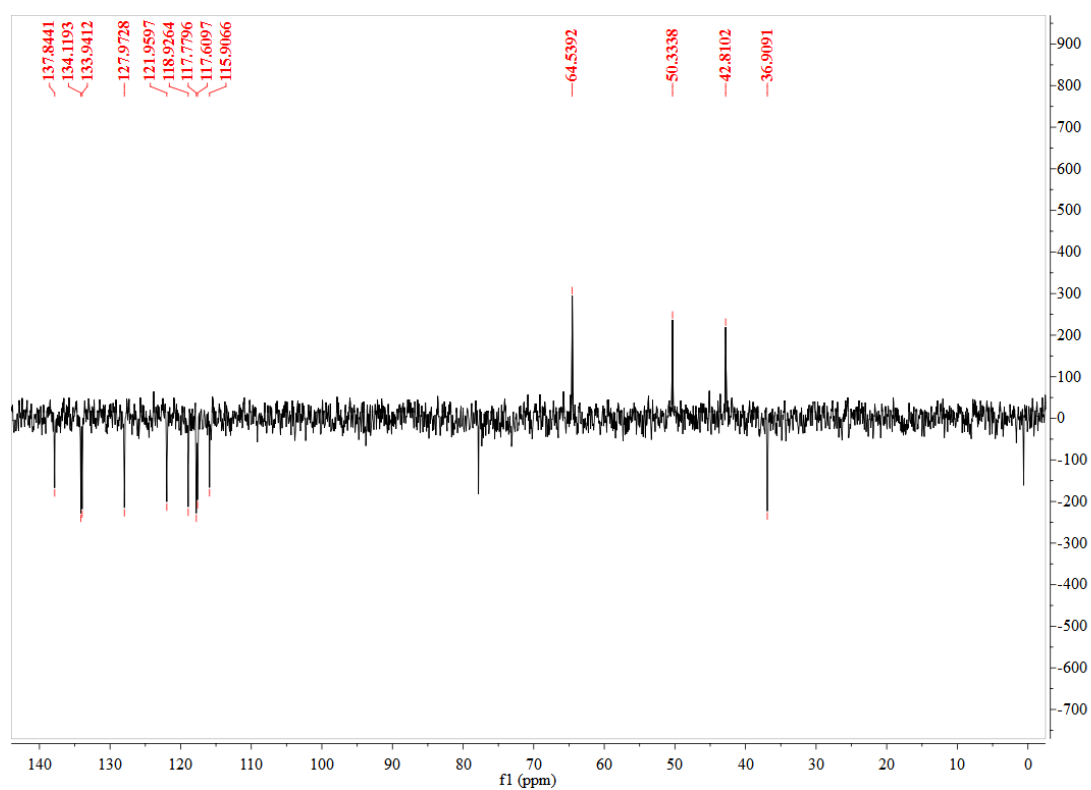


**Figure S31.** DEPT spectrum of dalescone B (**14**,  $\text{CDCl}_3$ ).

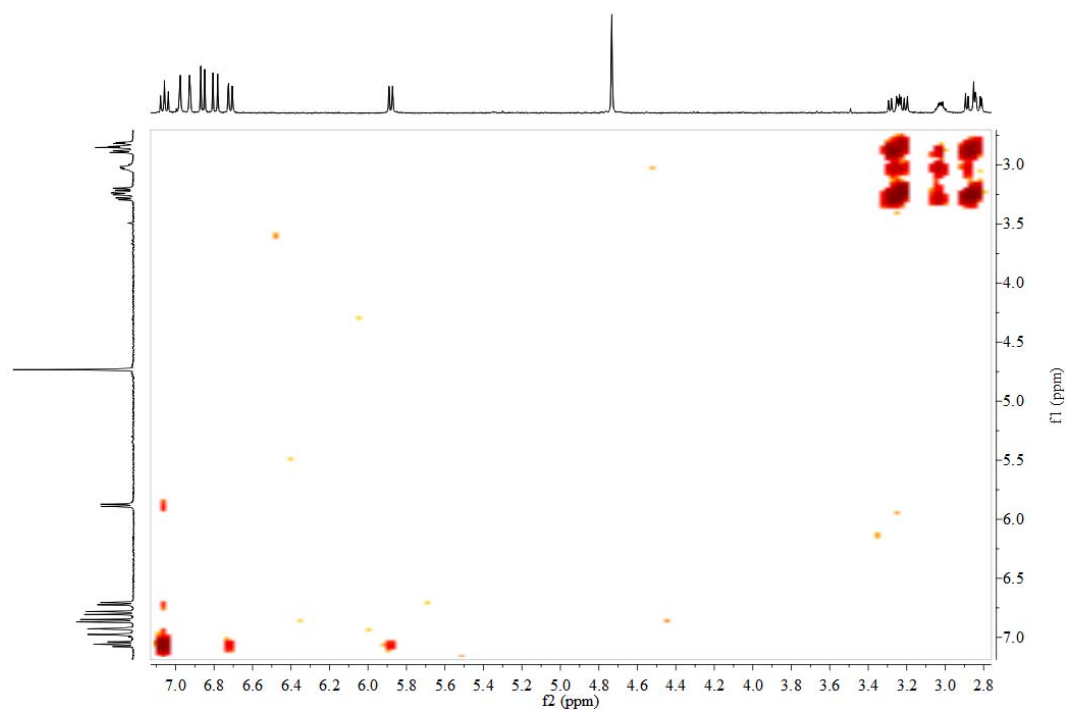


**Figure S32.**  $^1\text{H}$ - $^1\text{H}$  COSY spectrum of dalescone B (**14**,  $\text{CDCl}_3$ ).

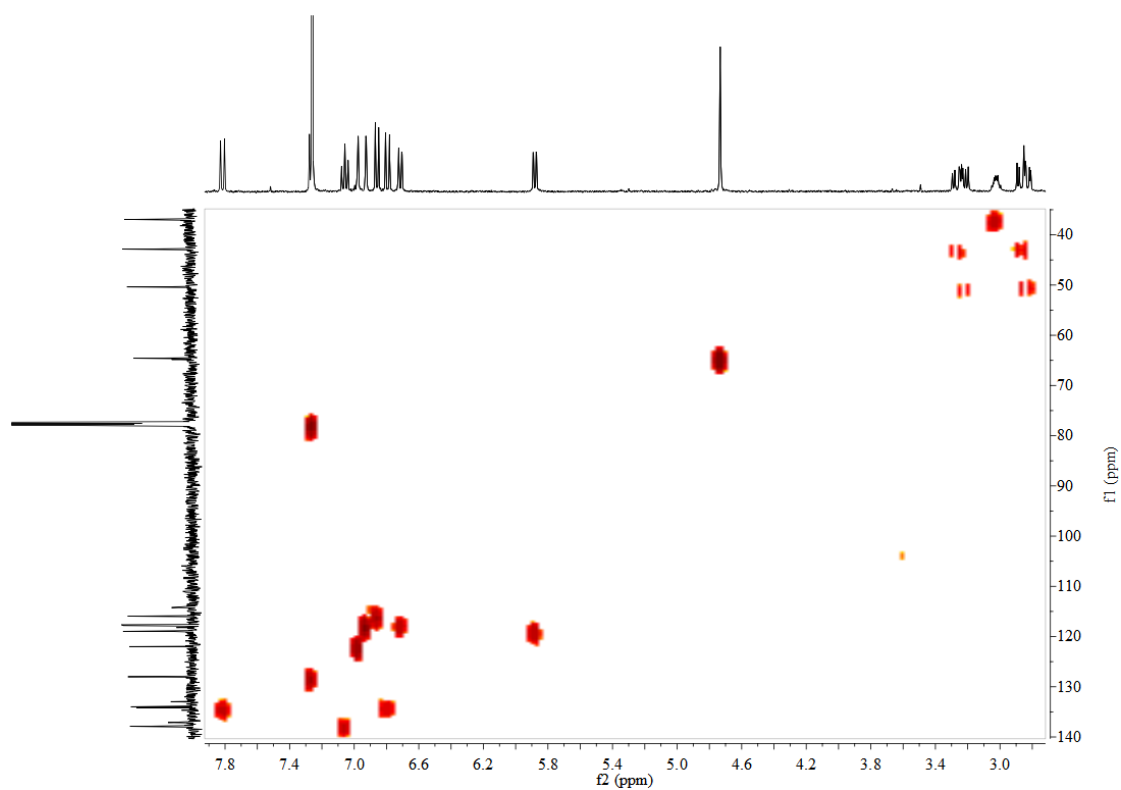


**Figure S33.** HSQC spectrum of dalescone B (**14**, CDCl<sub>3</sub>).

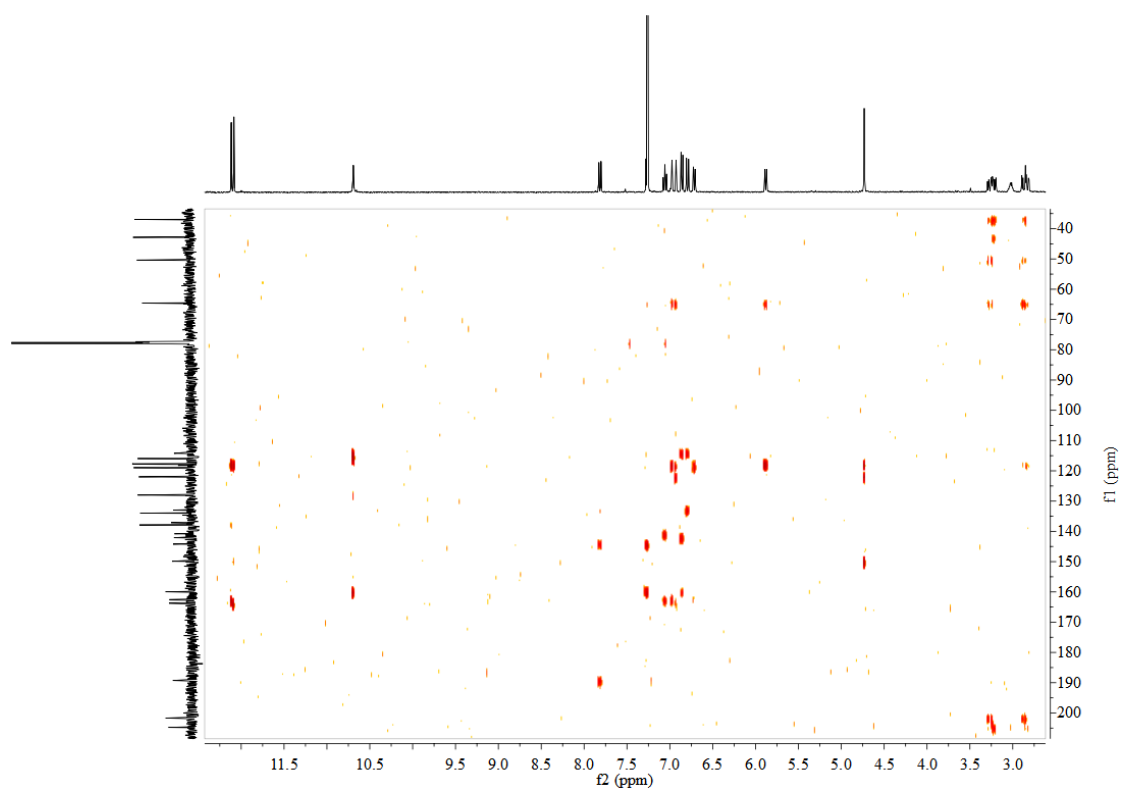


**Figure S34.** HMBC spectrum of dalescone B (**14**, CDCl<sub>3</sub>).

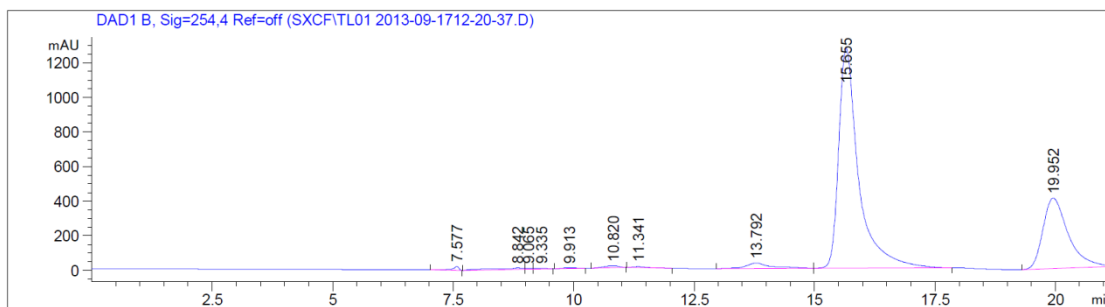


**Figure S35.** Chiral HPLC separation of dalescone C (**15**).

<Column Performance Report>

Column: CHIRALPAK® IA™, 0.50 cm ID. × 25 cm L, 5 μm

Mobile Phase: DCM/MeOH = 10/90 (v/v)

Peak No.	Time	Area	Area %
1	15.655	36695	68.0719
2	19.952	14846	27.5405

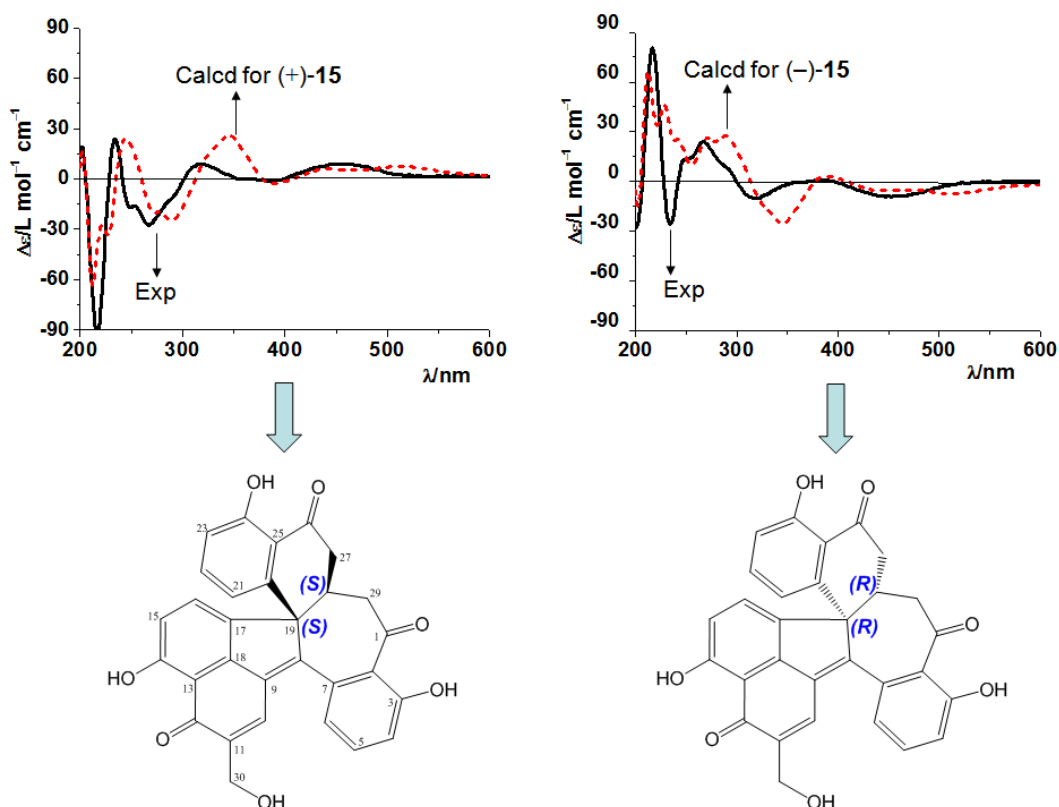


**Figure S36.** Absolute configurations of (+)- and (-)-**15** by comparing the experimental and calculated ECD spectra.



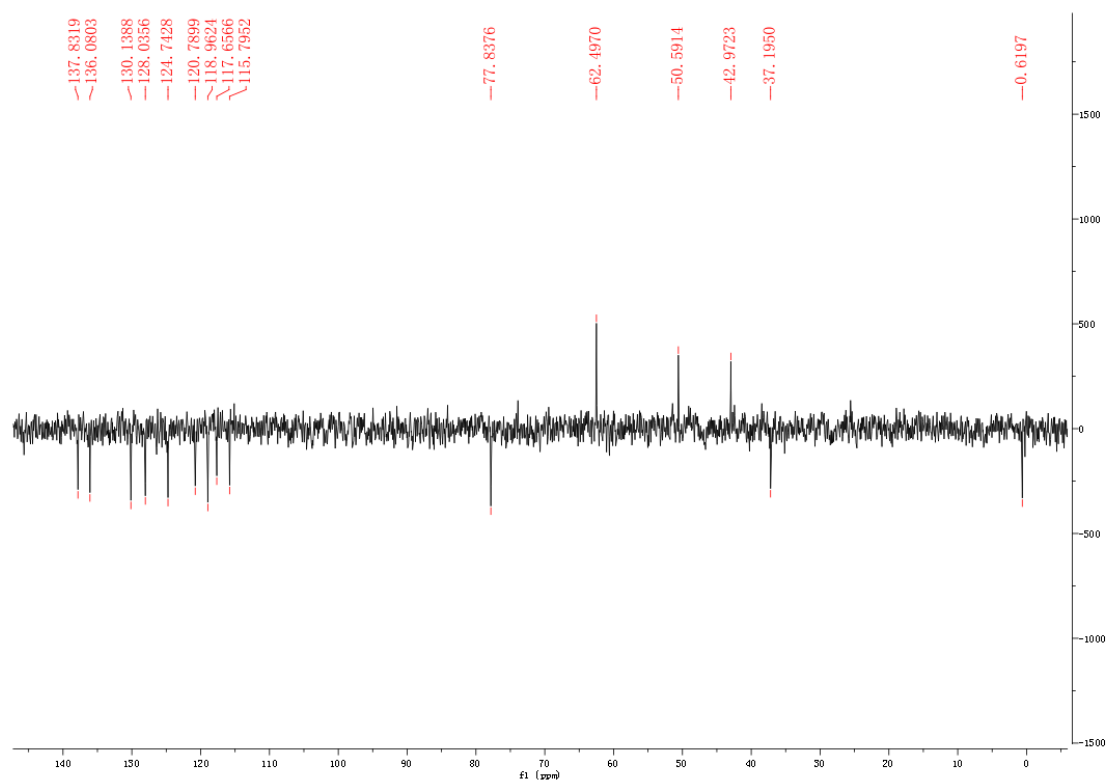


**Figure S39.** DEPT spectrum of dalescone C (**15**, CDCl<sub>3</sub>).

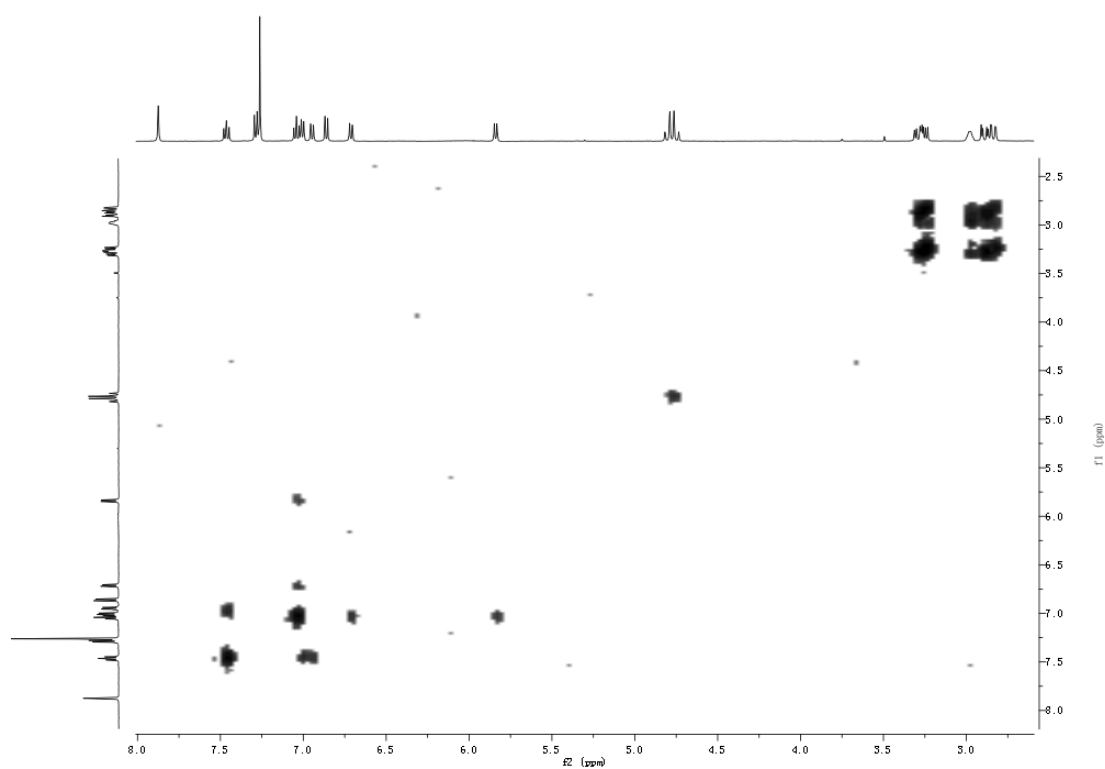


**Figure S40.** <sup>1</sup>H-<sup>1</sup>H COSY spectrum of dalescone C (**15**, CDCl<sub>3</sub>).

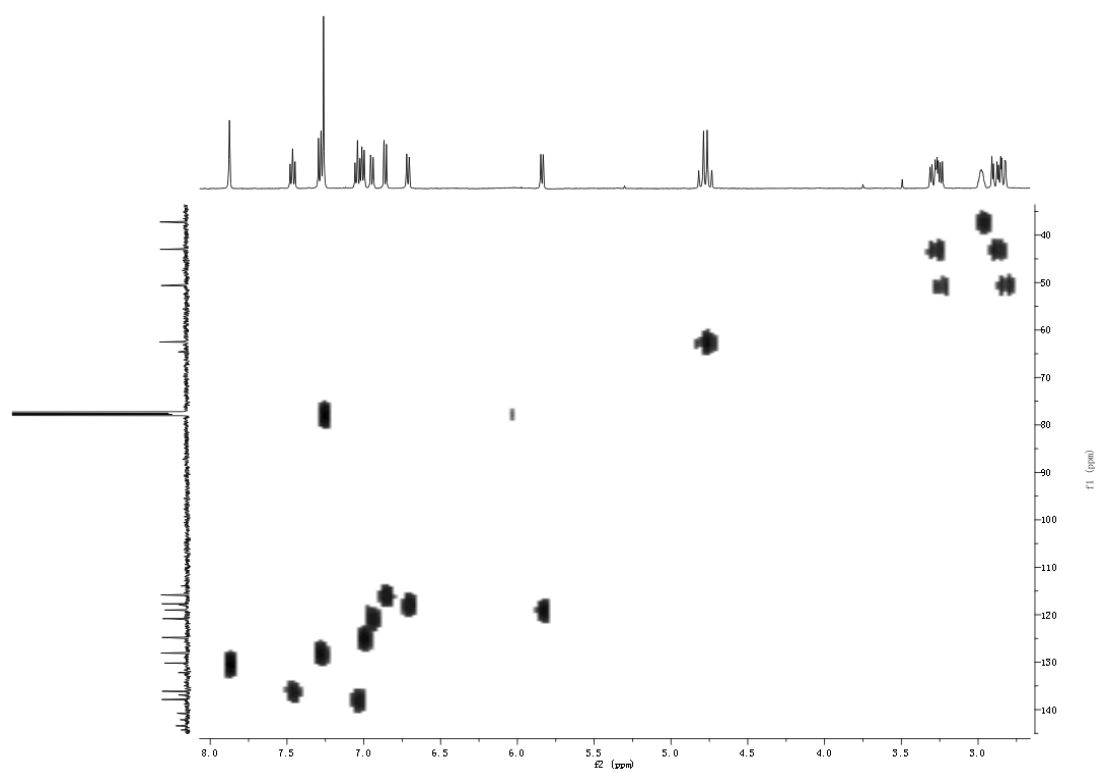


**Figure S41.** HSQC spectrum of dalescone C (**15**, CDCl<sub>3</sub>).

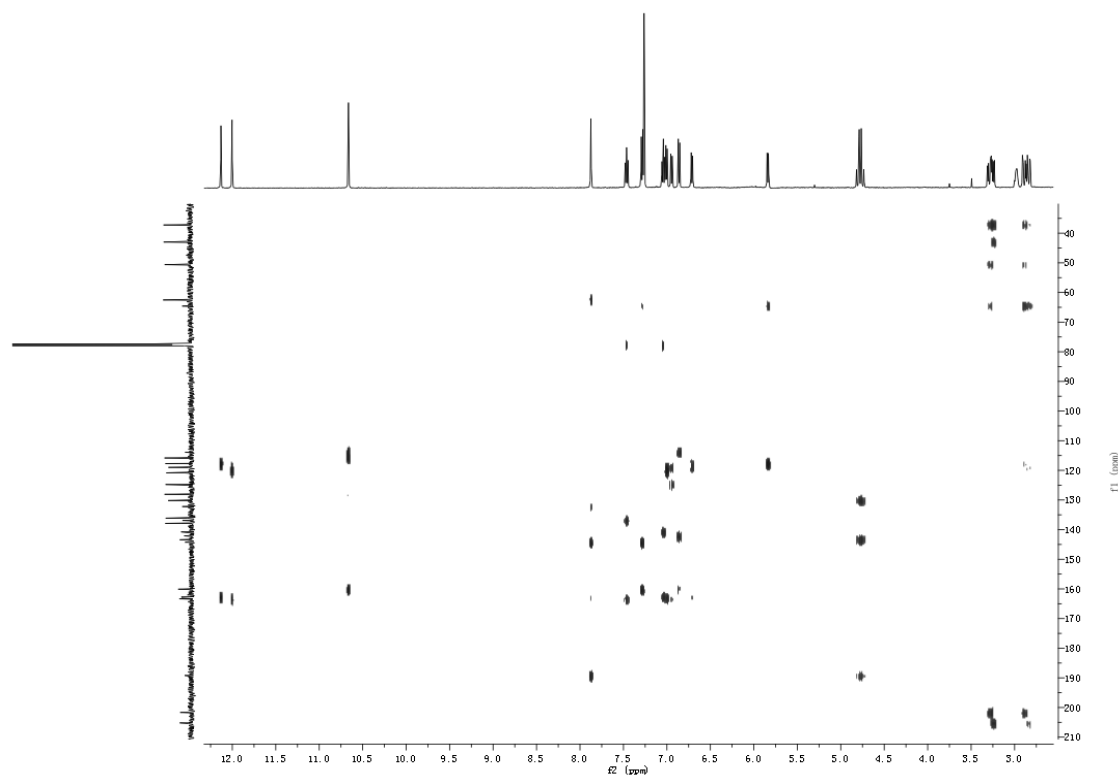


**Figure S42.** HMBC spectrum of dalescone C (**15**, CDCl<sub>3</sub>).



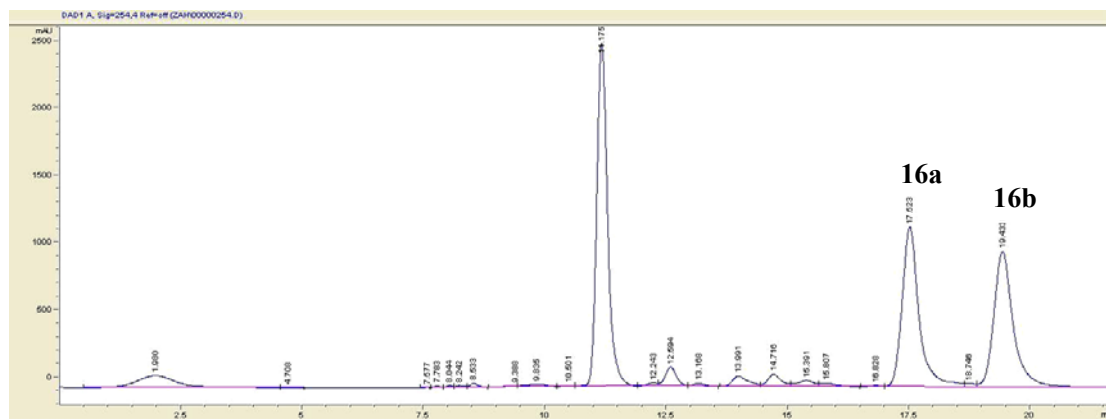


**Figure S43.** Semi-preparative HPLC separation of dalescone D (**16a**) and dalescone D (**16b**).

<Column Performance Report>

Column: Thermo Hypersil ODS-2, 0.50 cm ID. × 25 cm L, 5 μm

Mobile Phase: MeOH/H<sub>2</sub>O = 75/25 (v/v)

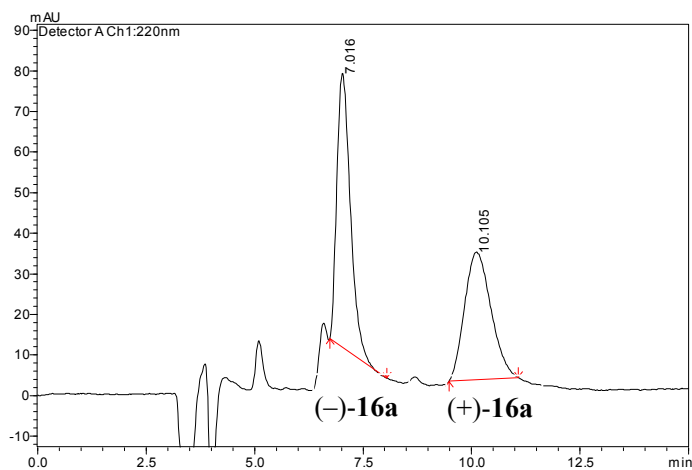


**Figure S44.** Chiral HPLC separation of dalescone D (**5a**).

<Column Performance Report>

Column: CHIRALPAK<sup>®</sup> OJ-H<sup>™</sup>, 0.46 cm ID. × 25 cm L

Mobile Phase: MeOH/HAC=100/0.1 (v/v)

Peak No.	Time	Area	Area %
1	7.016	1466	52.4288
2	10.105	1330	47.5712

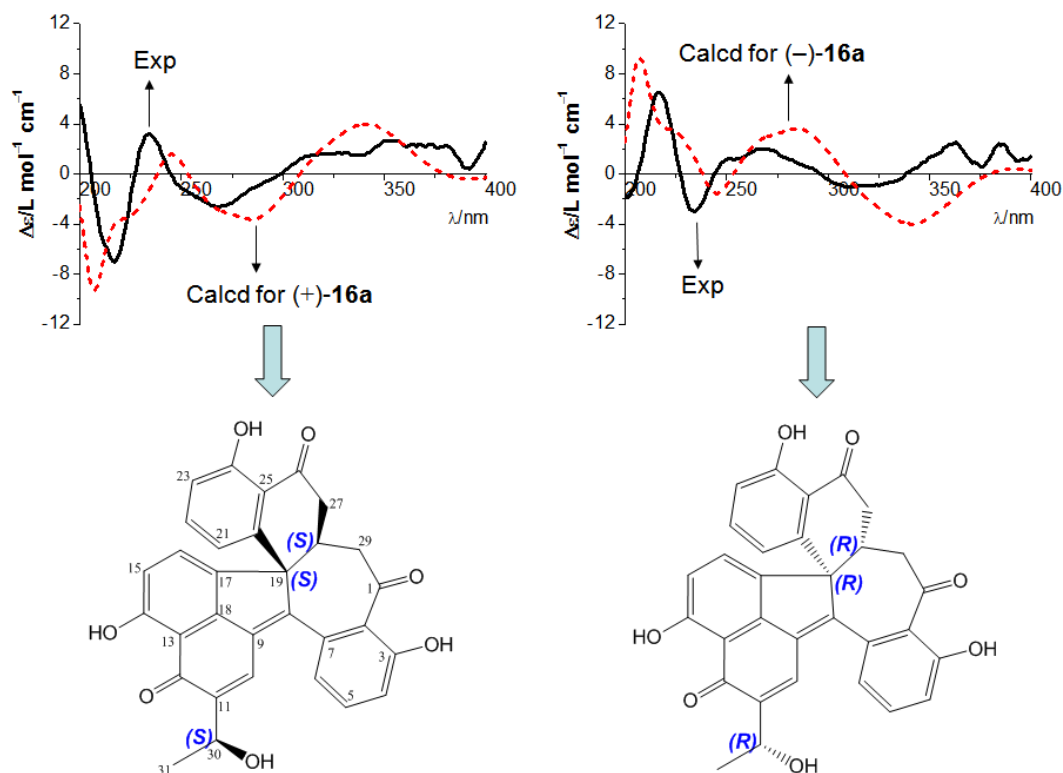


**Figure S45.** Absolute configurations of (+)- and (-)-**16a** by comparing the experimental and calculated ECD spectra.

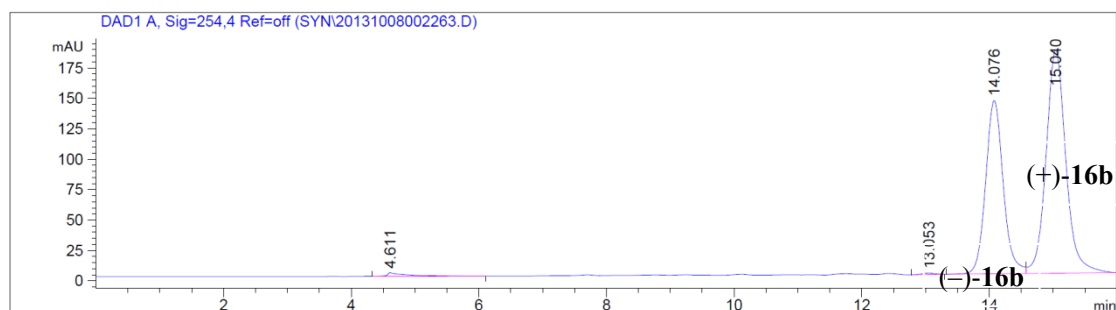


**Figure S46.** Chiral HPLC separation of dalescone D (**16b**).

<Column Performance Report>

Column: CHIRALPAK<sup>®</sup> IA<sup>™</sup>, 0.50 cm ID. × 25 cm L, 5 μm

Mobile Phase: DCM/MeOH = 20/80 (v/v)

Peak No.	Time	Area	Area %
1	14.076	2735	40.4243
2	15.040	3950	58.3777

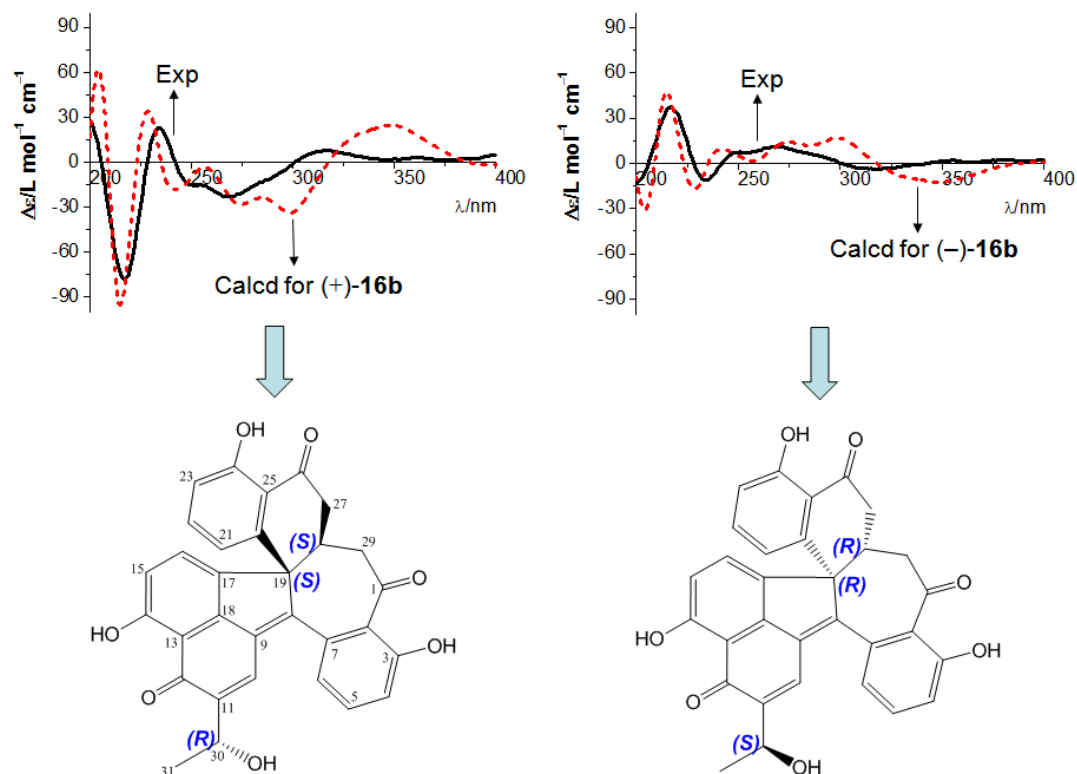


**Figure S47.** Absolute configurations of (+)- and (-)-16b by comparing the experimental and calculated ECD spectra.

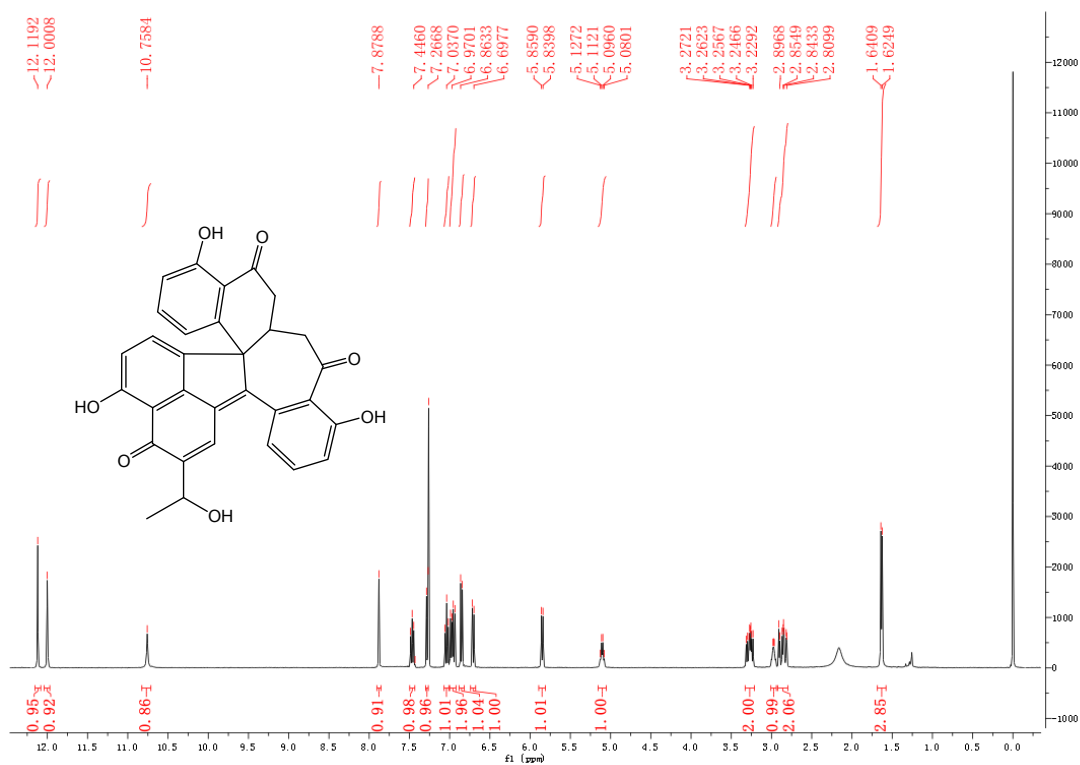


**Figure S48.**  $^1\text{H}$ -NMR spectrum of dalescone D (16, 400 MHz,  $\text{CDCl}_3$ ).

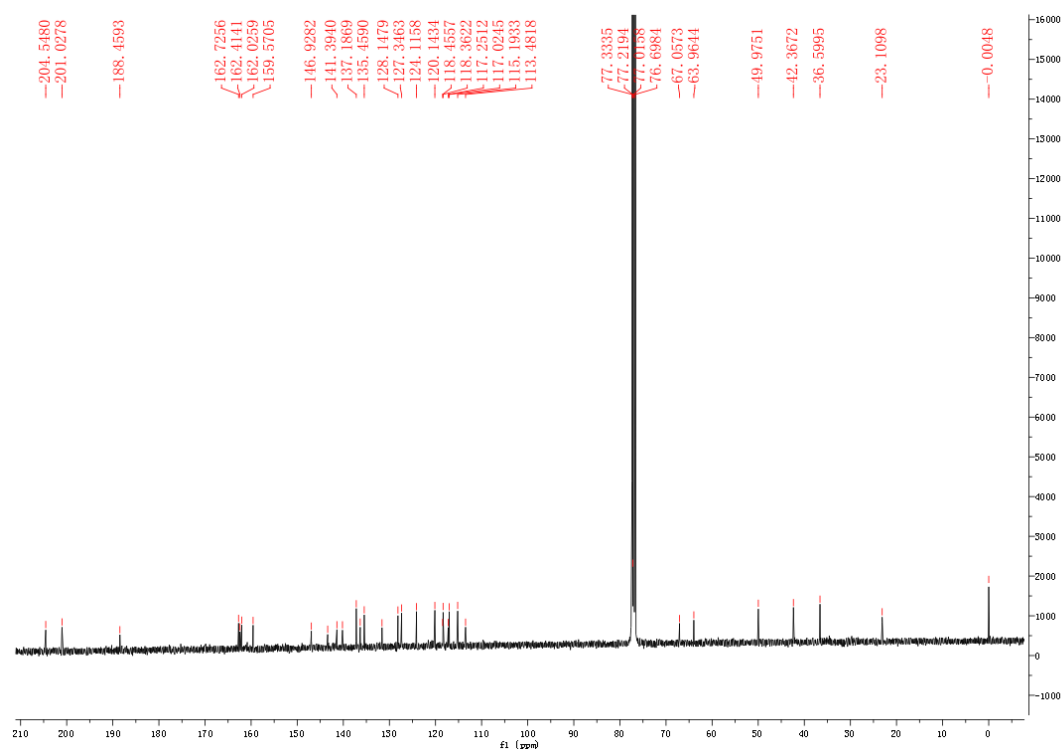


**Figure S49.**  $^{13}\text{C}$ -NMR spectrum of dalescone D (**16**, 100 MHz,  $\text{CDCl}_3$ ).

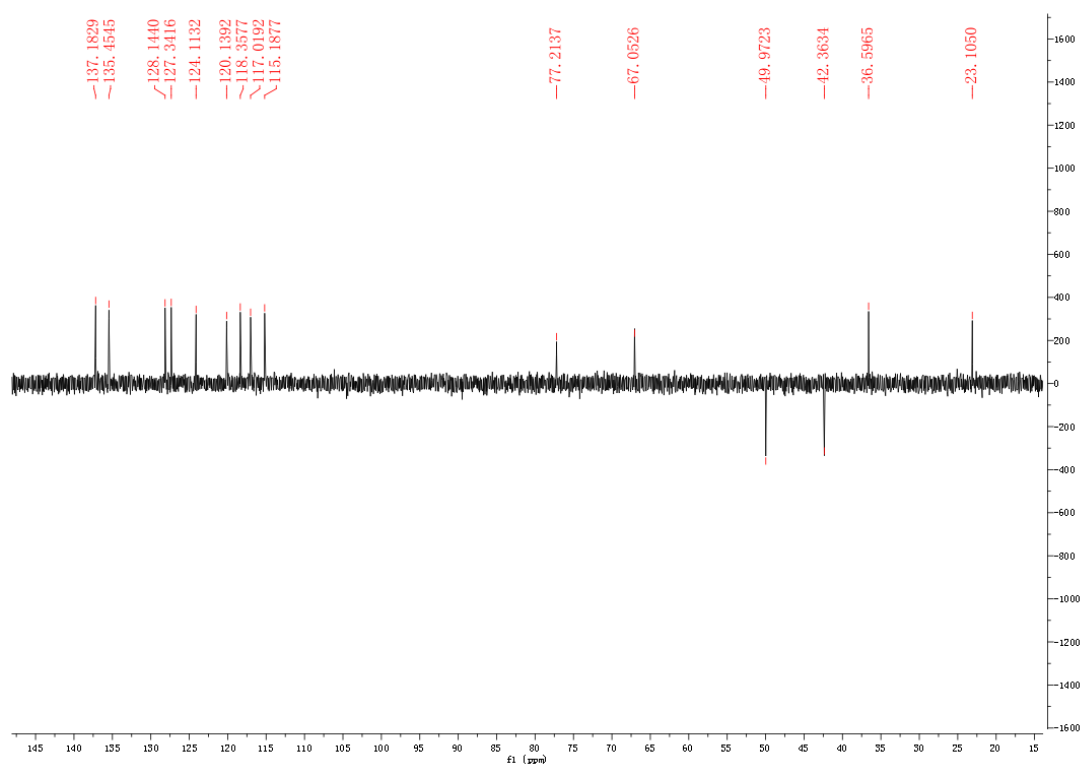


**Figure S50.** DEPT spectrum of dalescone D (**16**,  $\text{CDCl}_3$ ).

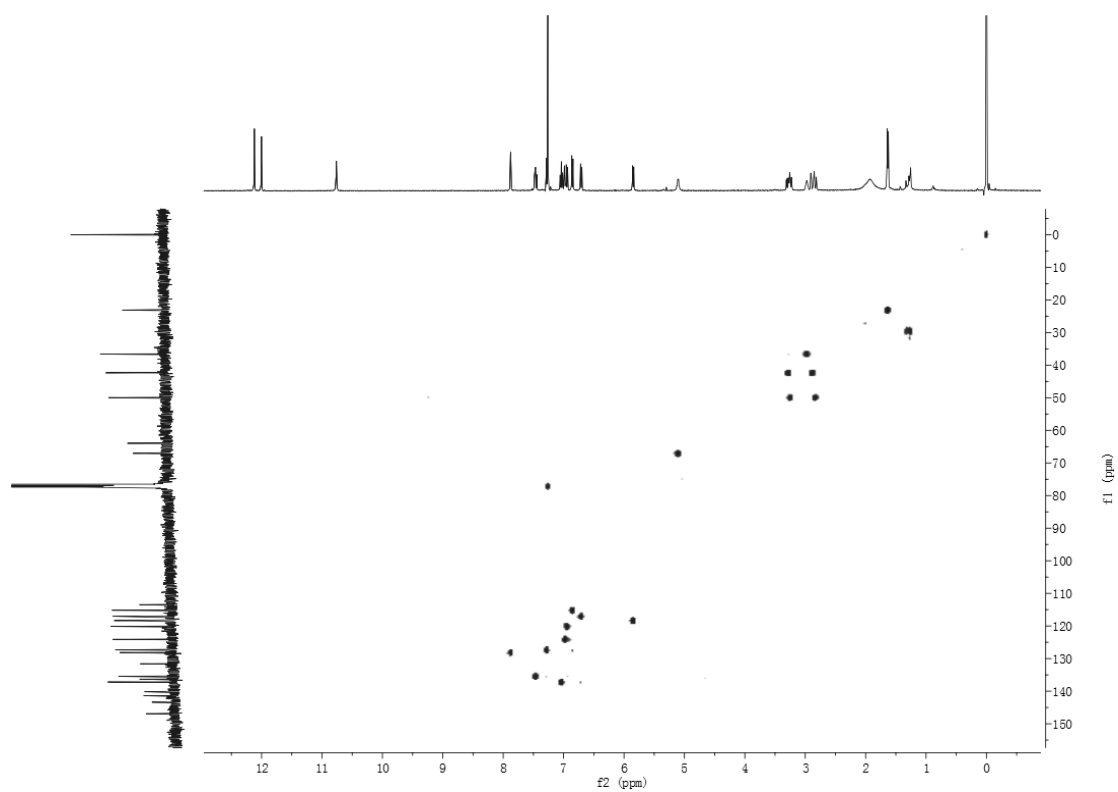


**Figure S51.** HSQC spectrum of dalescone D (**16**, CDCl<sub>3</sub>).

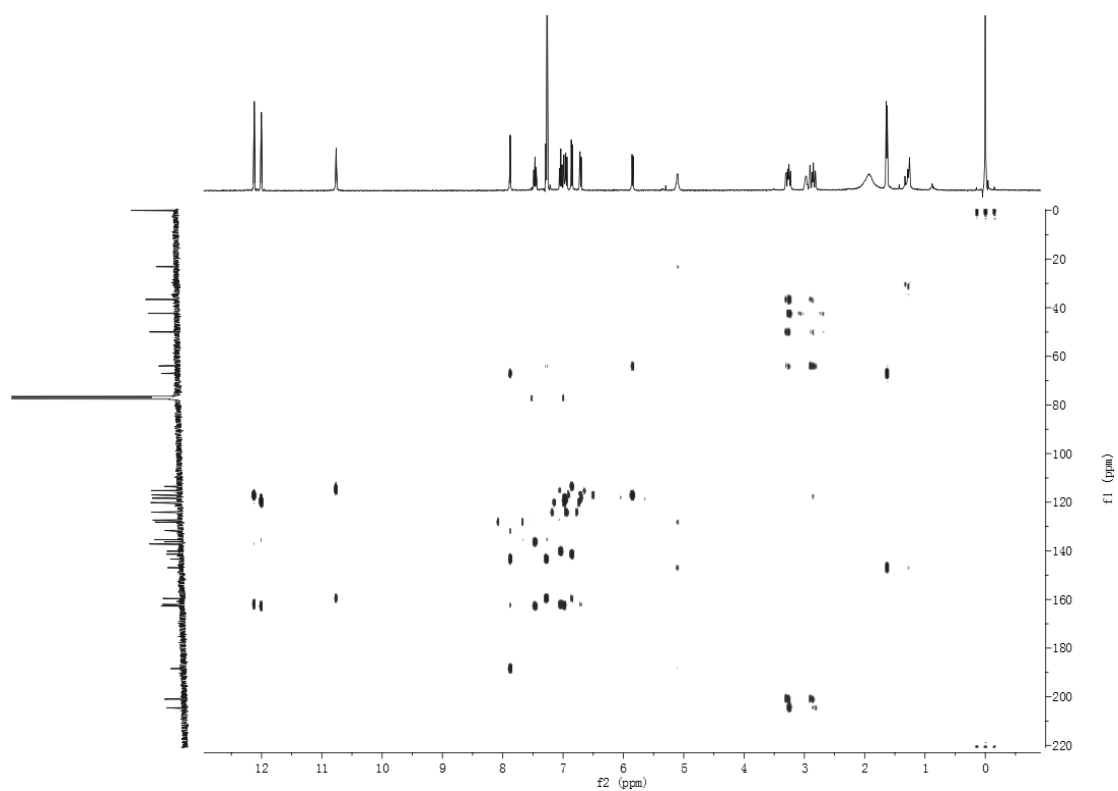


**Figure S52.** HMBC spectrum of dalescone D (**16**, CDCl<sub>3</sub>).

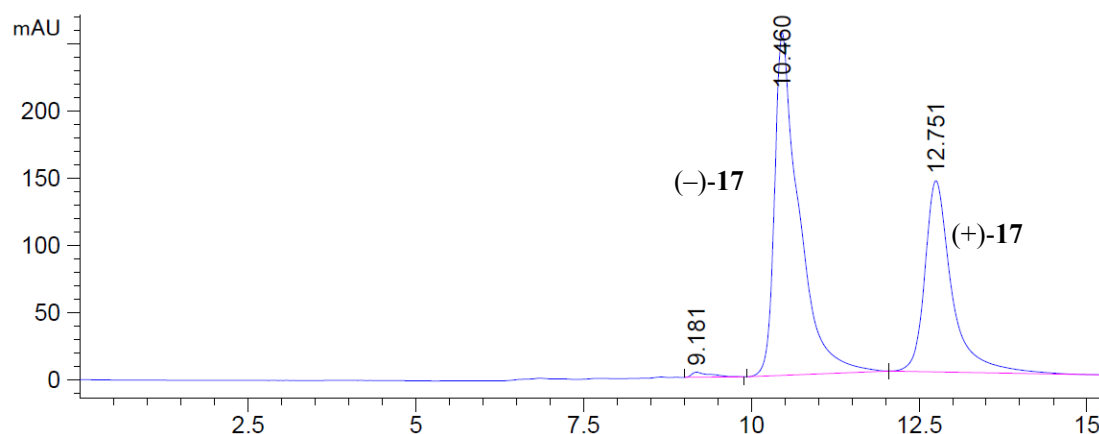


**Figure S53.** Chiral HPLC separation of dalescone E (**17**).

<Column Performance Report>

Column: CHIRALPAK® IA™, 0.50 cm ID. × 25 cm L, 5 μm

Mobile Phase: DCM/EtOH = 10/90 (v/v)

Peak No.	Time	Area	Area %
1	10.460	6447	59.9241
2	12.751	3991	37.0921

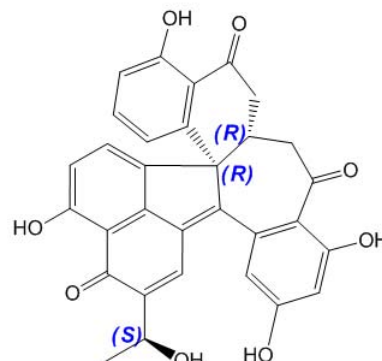
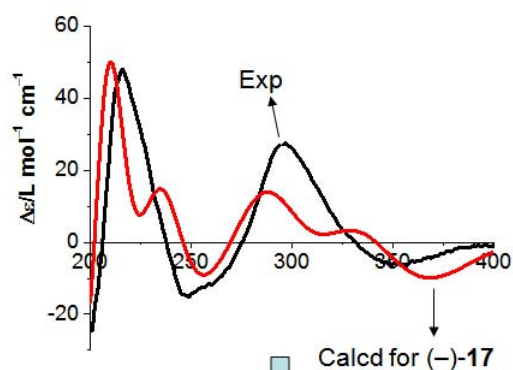
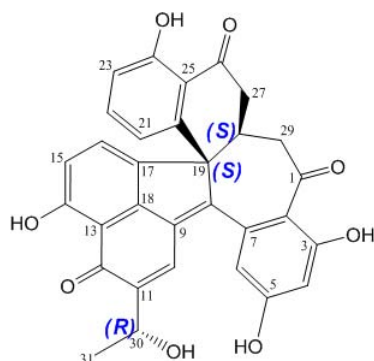
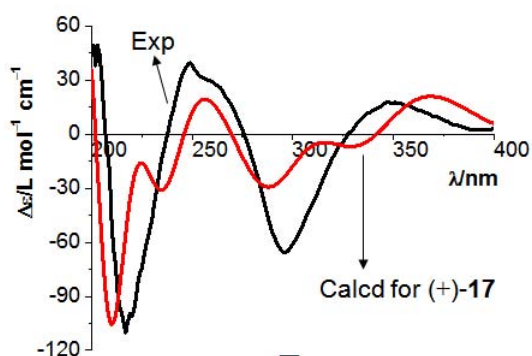


**Figure S54.** Absolute configurations of (+)- and (-)-**17** by comparing the experimental and calculated ECD spectra.

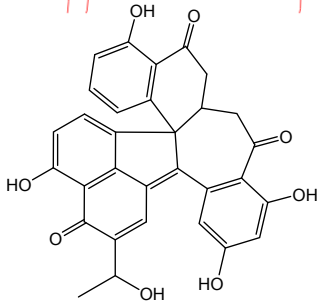




**Figure S57.**  $^{13}\text{C}$ -NMR spectrum of dalescone E (**17**, 125 MHz,  $\text{CDCl}_3$ ).

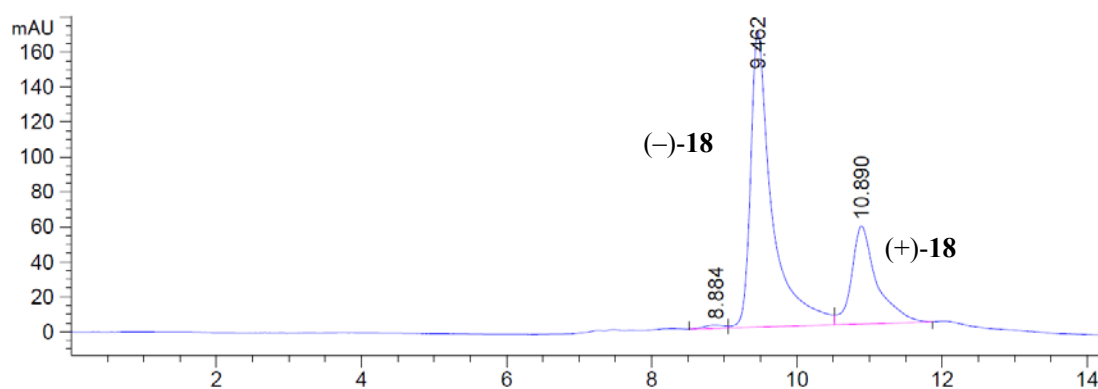


**Figure S58.** Chiral HPLC separation of dalescone F (**18**).

<Column Performance Report>

Column: CHIRALPAK<sup>®</sup> IA<sup>™</sup>, 0.50 cm ID. × 25 cm L, 5  $\mu\text{m}$

Mobile Phase: DCM/EtOH = 20/80 (v/v)

Peak No.	Time	Area	Area %
1	9.462	3479	71.4998
2	10.890	1351	27.7652



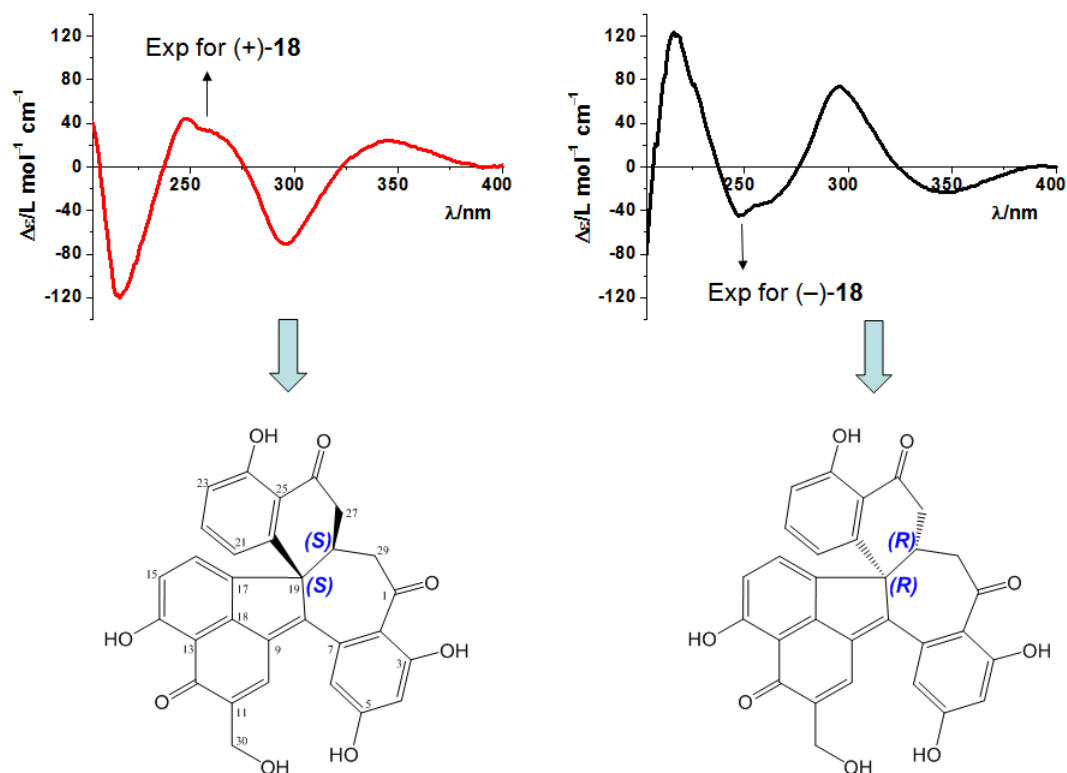


**Figure S59.** Absolute configurations of (+)- and (-)-**16b** by comparing the experimental and calculated ECD spectra.

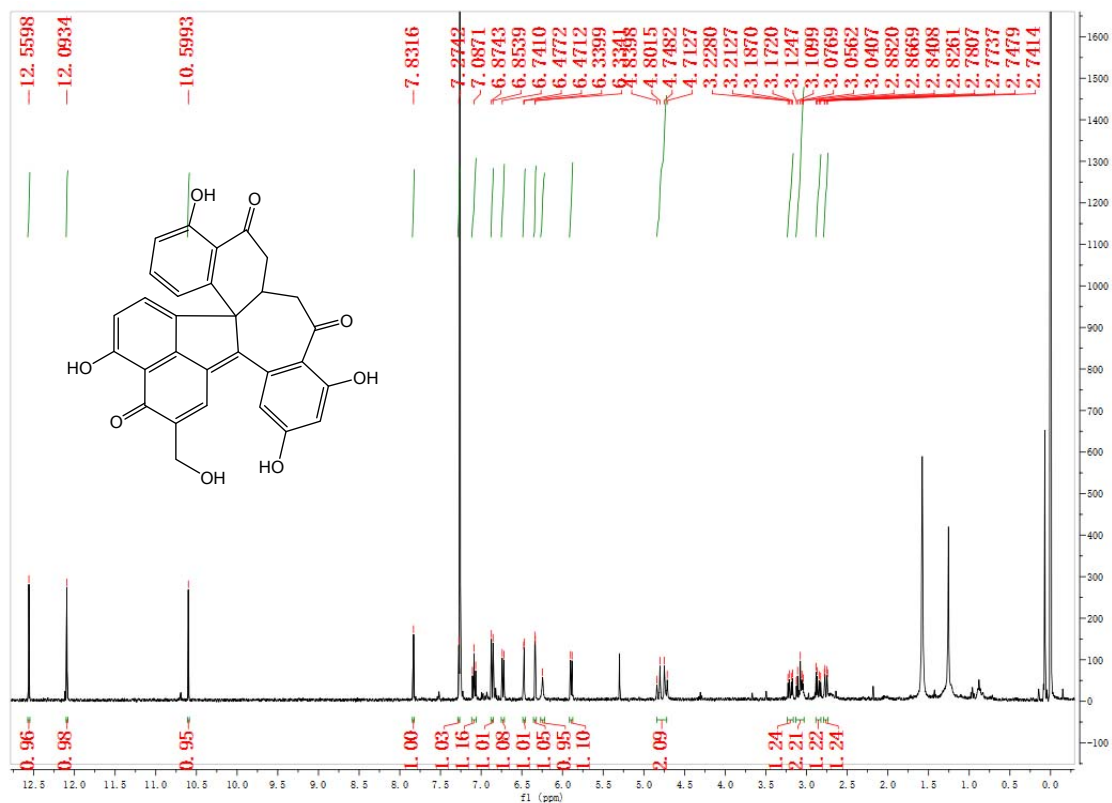


**Figure S60.** <sup>1</sup>H-NMR spectrum of dalescone F (**18**, 400 MHz, CDCl<sub>3</sub>).

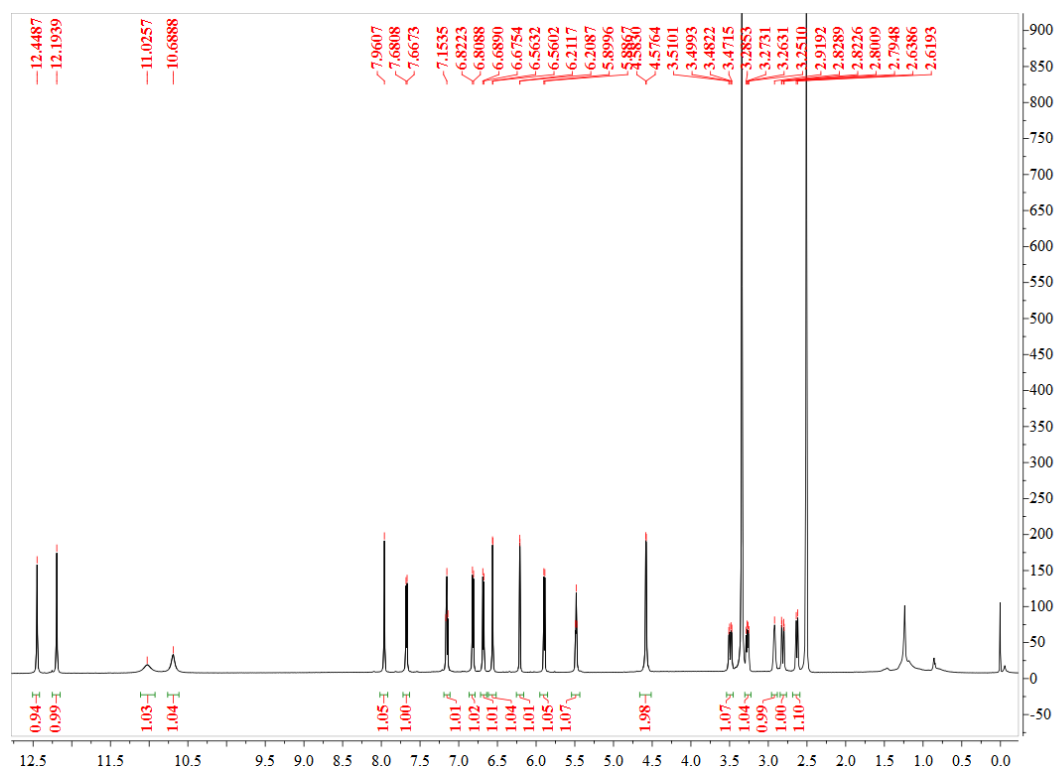


**Figure S61.** <sup>1</sup>H-NMR spectrum of dalescone F (**18**, 600 MHz, DMSO-*d*<sub>6</sub>).

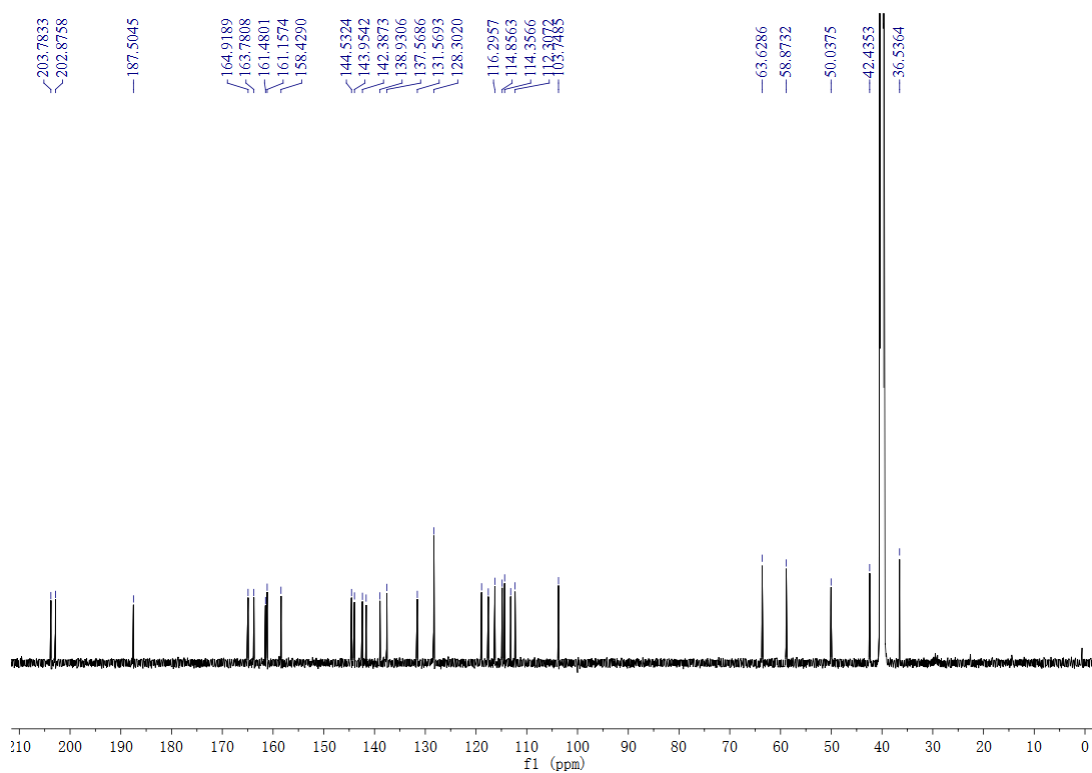


**Figure S62.** <sup>13</sup>C-NMR spectrum of dalescone F (**18**, 125 MHz, DMSO-*d*<sub>6</sub>).

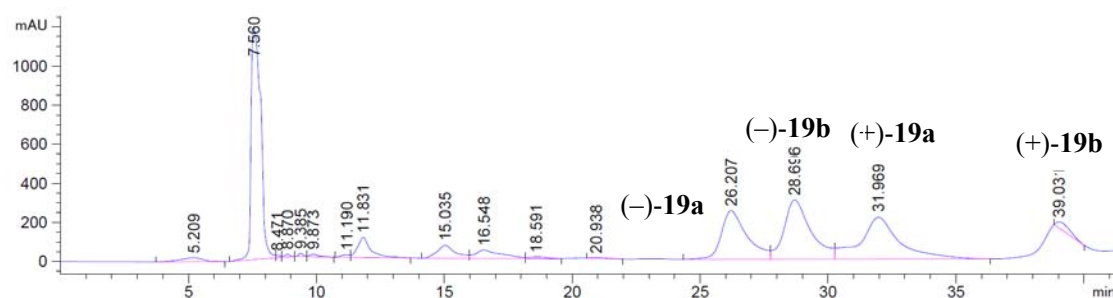


**Figure S63.** Chiral HPLC separation of dalescone G (**19**).

<Column Performance Report>

Column: CHIRALPAK<sup>®</sup> IA<sup>™</sup>, 0.50 cm ID. × 25 cm L, 5 μm

Mobile Phase: EtOH = 100 (v)

Peak No.	Time	Area	Area %
1	26.207	258	19.7473
2	28.696	281	21.5073
3	31.969	269	20.5527
4	39.031	254	19.4278

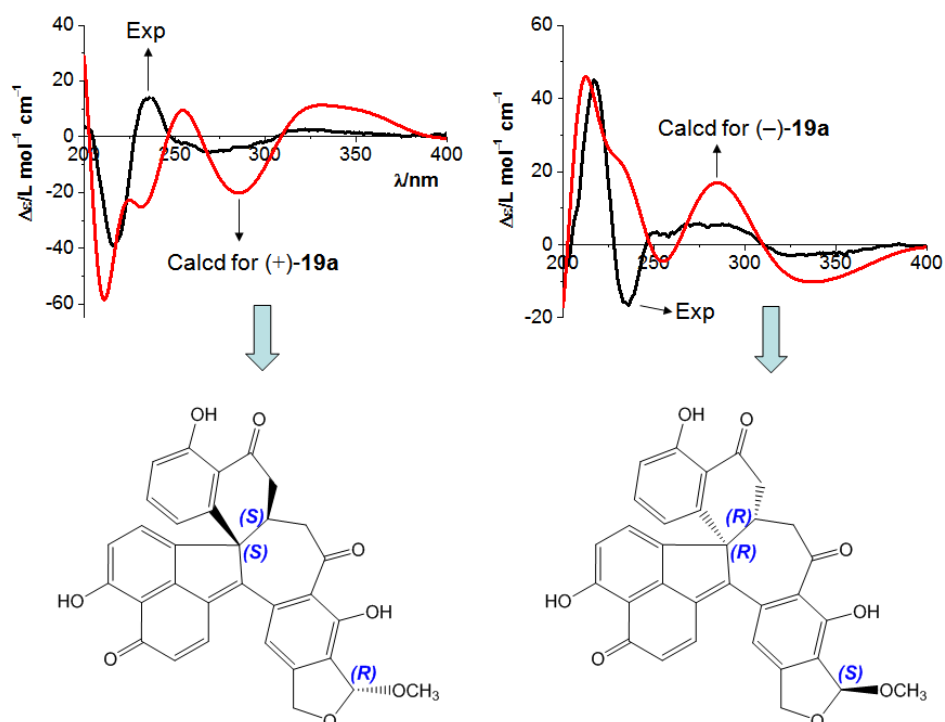


**Figure S64.** Absolute configurations of (+)- and (-)-**19a** by comparing the experimental and calculated ECD spectra.

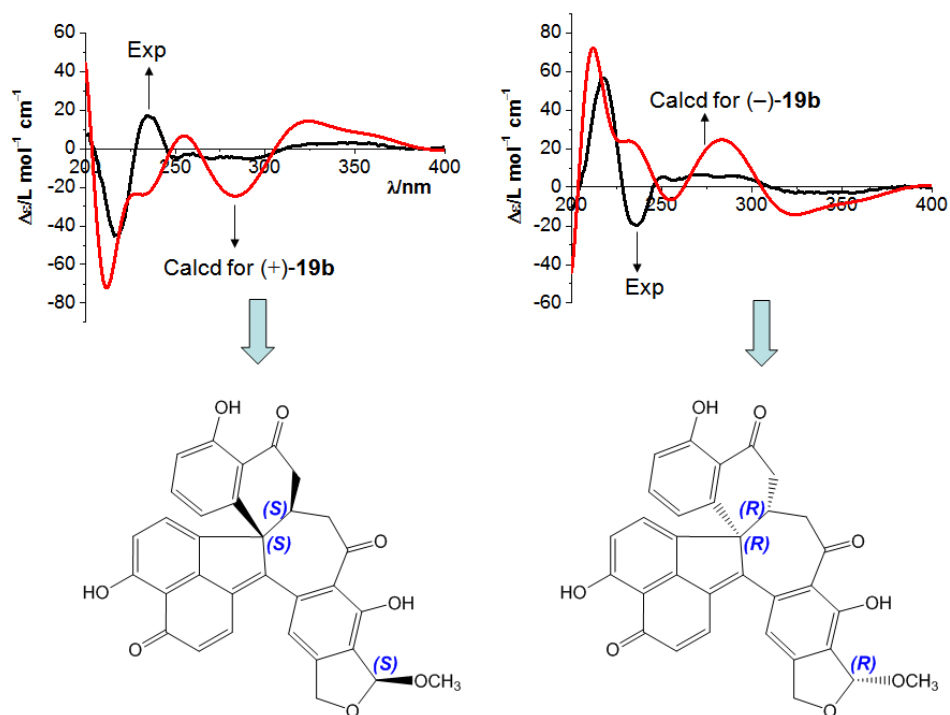


**Figure S65.** Absolute configurations of (+)- and (-)-19b by comparing the experimental and calculated ECD spectra.

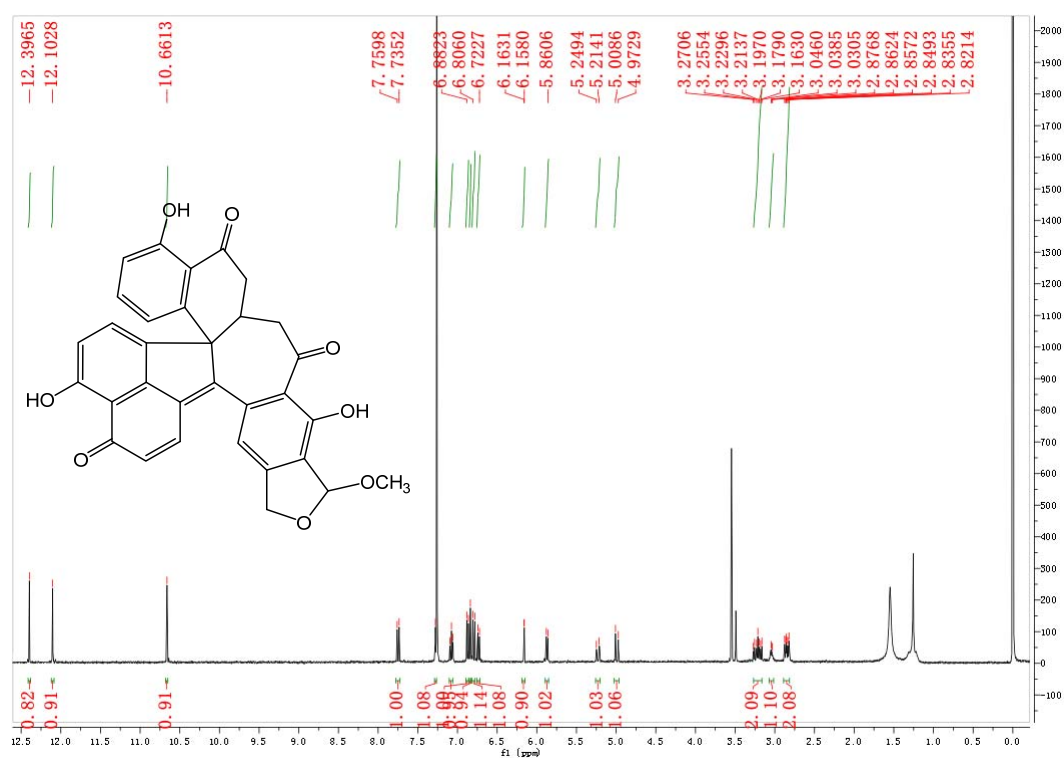


**Figure S66.**  $^1\text{H}$ -NMR spectrum of dalescone G (19, 400 MHz,  $\text{CDCl}_3$ ).